UNIVERSIDAD DE CONCEPCION
PROGRAMAS DE POSTGRADO

PROGRAMA MAGISTER EN CIENCIAS FORESTALES

Evaluación de nanocristales de celulosa polimorfos desde pulpa de eucalipto en el desarrollo de un material biobasado con ácido poliláctico

Cristóbal Alejandro Donoso Riquelme
CONCEPCIÓN - CHILE
2026

Profesor Guía: Dr. Regis Teixeira Mendonça
Laboratorio de Biopolímeros y Materiales Biobasados
Centro de Biotecnología, Universidad de Concepción

EVALUACIÓN DE NANOCRISTALES DE CELULOSA POLIMORFOS DESDE PULPA DE EUCALIPTO EN EL DESARROLLO DE UN MATERIAL BIOBASADO CON ÁCIDO POLILÁCTICO

Profesor Guía	Regis Marcelo Teixeira Mendonça Profesor Titular Ingeniero Químico, Dr.
Profesor Co-Guía	María Graciela Aguayo Palma Colaboradora Académica Ingeniera de Ejecución en Maderas, Dr.

AGRADECIMIENTOS

Quisiera agradecer en primer lugar a mi profesor guía, Dr. Regis Teixeira Mendonça, por darme la oportunidad de desarrollar esta investigación bajo su orientación y por su constante apoyo académico a lo largo de este proceso. A mi colega Isidora Reyes por enseñarme sus conocimientos en el área y apoyo durante toda esta etapa.

Al Proyecto Fondecyt Regular 1231086 por el financiamiento que hizo posible el desarrollo de esta tesis, y a la Facultad de Ciencias Forestales y a la Dirección de Postgrado de la Universidad de Concepción por la beca de articulación pregrado-postgrado y financiamiento para la pasantía de investigación en Auburn University, Estados Unidos.

A la Dra. María Soledad Peresin y al Sustainable Bio-Based Materials Laboratory por la acogida y el apoyo durante la pasantía. Un agradecimiento especial a Dúber Garcés y Diego Cuartas, por su amistad y compañía durante esa etapa.

A mis padres, Fidel y Kateryne, por inculcarme con amor, comprensión y perseverancia el valor de perseguir nuevos desafíos. A toda mi familia, abuelos y hermanos, por su apoyo incondicional y por estar siempre presentes.

A todas mis amistades y colegas que me impulsan a ser mejor cada día.

Muy agradecido por el apoyo de todas las personas que me han acompañado a lo largo de este camino, ahora más que nunca.

Gracias,

TABLA DE CONTENIDOS

ÍNDICE DE TABLAS

ÍNDICE DE FIGURAS

RESUMEN

Poliácido láctico (PLA) es un polímero biodegradable prometedor, pero su baja velocidad de cristalización, fragilidad y modesta estabilidad térmica limitan su uso en aplicaciones de envases de alto desempeño. Los nanocristales de celulosa (CNC) son refuerzos nanométricos de origen biobasado atractivos; sin embargo, su carácter hidrofílico dificulta la compatibilidad con matrices de PLA hidrofóbicas. En este trabajo, se produjeron CNC derivados de las formas polimórficas I y II de la celulosa a partir de pulpa kraft blanqueada de eucalipto, se acetilaron bajo condiciones heterogéneas idénticas y se incorporaron como nanorefuerzos en filmes biocompuestos de PLA obtenidos por colado en disolución, a contenidos de 0,5; 1,0 y 1,5% p/p. Los CNC del polimorfismo tipo II alcanzaron un grado de sustitución significativamente mayor (1,38) que los de tipo I (0,23), evidenciando la mayor accesibilidad química de la forma regenerada. Al incorporarse en los filmes de PLA, los nanocristales basados en celulosa II actuaron como agentes de nucleación más eficientes que la celulosa I, con índices de cristalinidad por XRD que alcanzaron hasta 44,20% para PLA/ACNC II al 1,5% p/p, en comparación con 13,32% para PLA puro. El análisis por DSC confirmó esta tendencia, observándose un incremento del grado de cristalinidad (Xc) desde 27,33% en PLA puro hasta 98,26% en PLA/CNC II al 1,5% p/p. Estas mejoras en la cristalinidad de la matriz se acompañaron de una mayor estabilidad térmica, donde PLA/ACNC II 1,5% p/p presentó un Tonset de 330,7 °C y un Tmax de 357,8 °C, lo que representa aumentos de aproximadamente 16 °C y 13 °C con respecto a PLA puro, atribuidos a la desulfatación parcial y a la hidrofobización superficial inducidas por la acetilación. Los ensayos mecánicos mostraron que los CNC y ACNC, en general, mantuvieron o incrementaron ligeramente la resistencia a la tracción y el módulo de Young en relación con el PLA puro; sin embargo, la alta dispersión de los datos a mayores contenidos sugirió una transferencia de esfuerzos limitada por la aglomeración. En conjunto, los nanocristales de celulosa acetilados de tipo II se perfilan como cargas nucleantes superiores para biocompuestos de PLA, siendo el intervalo de carga de 0,5–1,0% p/p el que ofrece el equilibrio más favorable entre cristalinidad aumentada, estabilidad térmica y desempeño mecánico esencialmente preservado para aplicaciones de envases sostenibles.

ABSTRACT

Polylactic acid (PLA) is a promising biodegradable polymer whose low crystallization rate, brittleness, and modest thermal stability limit its use in high-performance packaging applications. Cellulose nanocrystals (CNCs) are attractive bio-based nanoreinforcements; however, their hydrophilic character hampers compatibility with hydrophobic PLA matrices. In this work, CNCs derived from cellulose polymorphs I and II were produced from bleached eucalyptus kraft pulp, acetylated under identical heterogeneous conditions, and incorporated as nanoreinforcements in solvent-cast PLA biocomposite films at loadings of 0.5, 1.0, and 1.5 wt%. CNCs of polymorph II yielded a markedly higher degree of substitution (1.38) than polymorph I (0.23), evidencing the greater chemical accessibility of the regenerated polymorph. When incorporated into PLA films, cellulose II-based nanocrystals acted as more efficient nucleating agents than their cellulose I-based, with XRD crystallinity indices reaching up to 44.20% for PLA/ACNC II at 1.5 wt%, compared to 13.32% for neat PLA. DSC analysis confirmed this trend, with the degree of crystallinity (Xc) increasing from 27.33% in neat PLA to 98.26% in PLA/CNC II at 1.5 wt%. These improvements in matrix crystallinity were accompanied by enhanced thermal stability, with PLA/ACNC II 1.5 wt% exhibiting a Tonset of 330.7 °C and a Tmax of 357.8 °C, representing increases of approximately 16 °C and 13 °C relative to neat PLA, attributed to partial desulfation and surface hydrophobization induced by acetylation. Mechanical testing showed that CNCs and ACNCs generally maintained, and in some cases slightly increased, tensile strength and Young's modulus relative to neat PLA; however, high data dispersion at elevated loadings suggested agglomeration-limited stress transfer. Overall, acetylated cellulose nanocrystals of polymorph II emerge as superior nucleating fillers for PLA biocomposites, with a loading range of 0.5–1.0 wt% offering the most favorable balance between enhanced crystallinity, thermal stability, and essentially preserved mechanical performance for sustainable packaging applications.

I. ESTADO DEL ARTE

I.1. CRISIS GLOBAL DE PLÁSTICOS Y ECONOMÍA CIRCULAR

La acumulación de residuos plásticos derivados del petróleo representa uno de los desafíos ambientales más apremiantes del siglo XXI. Se estima que la producción mundial de plásticos superó los 400 millones de toneladas en 2023, y que menos del 10% del plástico generado en el mundo ha sido reciclado alguna vez. Gran parte de este flujo corresponde al sector del embalaje, que concentra aproximadamente el 40% del consumo total de plásticos. La persistencia de estos materiales en ecosistemas terrestres y marinos, con tiempos de degradación que pueden superar los 500 años, ha motivado iniciativas regulatorias a nivel global, incluyendo la directiva europea de plásticos de un solo uso y los compromisos adoptados en el marco del Tratado Global sobre Plásticos impulsado por la ONU (Melchor-Martínez et al., 2022).

En este contexto, la economía circular emerge como marco conceptual y operativo para reorientar el diseño, producción y gestión del fin de vida de los materiales. Los principios de la economía circular plantean sustituir los modelos lineales de extracción, uso y descarte por ciclos cerrados de reutilización, reciclaje y compostaje (Omran et al., 2021). Los bioplásticos, por definición corresponden a polímeros de origen biológico y/o biodegradables que se posicionan como una alternativa compatible con este enfoque, dado que pueden reducir la huella de carbono del embalaje y facilitar rutas de valorización al final de su vida útil (Agbakoba et al., 2023). El mercado global de embalajes con biopolímeros fue valorado en aproximadamente USD 23,5 mil millones en 2024 y se proyecta que crecerá a tasas superiores al 11% anual hasta 2030, impulsado principalmente por la demanda del sector alimentario y farmacéutico (Wi et al., 2025).

I.2. EL ÁCIDO POLILÁCTICO (PLA) COMO BIOPOLÍMERO PARA EMPAQUES

Entre los biopolímeros disponibles comercialmente, el ácido poliláctico (PLA) destaca por su origen renovable proveniente de la fermentación de almidones y azúcares, destaca por su capacidad de biodegradación en condiciones de

compostaje industrial. Sus propiedades mecánicas básicas, como la rigidez y la resistencia a la tracción, son comparables a las del poliestireno, lo que lo convierte en un candidato atractivo para aplicaciones de embalaje rígido y flexible (Dhar et al., 2017; Nofar et al., 2019). Sin embargo, el PLA presenta limitaciones intrínsecas que restringen su adopción a gran escala con una tasa de cristalización inherentemente lenta, baja tenacidad, permeabilidad relativamente elevada a gases como el CO_2 y el O_2, y una estabilidad térmica moderada que limita su procesabilidad industrial a temperaturas superiores a 150 °C (Vatansever et al., 2019).

Estas deficiencias están directamente relacionadas con la microestructura del PLA. En estado puro y fundido, el polímero solidifica preferentemente en una fase amorfa o semicristalina con índices de cristalinidad habitualmente bajos lo que explica su tenacidad y su baja resistencia al calor (Nofar et al., 2019). La incorporación de agentes nucleantes que son capaces de proporcionar sitios de nucleación durante la solidificación de los materiales es una de las estrategias para acelerar la cristalización del PLA, aumentando su cristalinidad y por consiguiente, mejorar su módulo de Young, estabilidad térmica y sus propiedades de barrera (Shin et al., 2022). En los últimos años, los nanocristales de celulosa han emergido como agentes nucleantes bio-basados con un potencial prometedor para esta aplicación (Bayat et al., 2025; Ryoo et al., 2025; Trivedi & Gupta, 2024).

I.3. NANOCRISTALES DE CELULOSA (CNCS) COMO NANOREFUERZOS BIO-BASADOS

La nanocelulosa, y en particular los nanocristales de celulosa (CNCs), ha concentrado una atención científica y tecnológica creciente durante la última década (Peng et al., 2021; Rashid et al., 2023). Los CNCs son nanoestructuras en forma de varillas altamente cristalinas, con anchuras típicas de 5 a 50 nm y longitudes de 100 a 500 nm, son obtenidos mediante hidrólisis ácida controlada de fuentes celulósicas como fibras de madera, algodón, bagazo o pulpa Kraft (Mariano et al., 2014). Su baja densidad, alta rigidez, biodegradabilidad y abundancia de grupos hidroxilo superficiales que permiten una amplia funcionalización química, los convierten en

candidatos atractivos para reforzar matrices poliméricas bio-basadas (Dufresne, 2019; Rana et al., 2021).

La extracción de CNCs a partir de pulpa Kraft de eucalipto es especialmente relevante en el contexto forestal chileno y latinoamericano. Chile es el tercer mayor exportador mundial de celulosa de eucalipto, con una capacidad instalada que supera los 3 millones de toneladas anuales (Carrillo-Varela et al., 2018). Las especies *Eucalyptus nitens* y *E. globulus* dominan las plantaciones forestales del centro-sur del país y constituyen la materia prima principal de la industria celulósica nacional. El aprovechamiento de residuos y subproductos de esta cadena productiva para la generación de nanomateriales representa una oportunidad de valorización de alto valor agregado, alineada con los objetivos de bioeconomía y desarrollo forestal sostenible (Reyes-González et al., 2024). Estudios previos han demostrado que la pulpa Kraft blanqueada de eucalipto permite obtener CNCs con altos índices de cristalinidad y morfología controlada mediante hidrólisis con ácido sulfúrico (Aguayo et al., 2020).

I.4. POLIMORFISMO; CELULOSA I Y CELULOSA II

Una característica fundamental de la celulosa que ha permanecido relativamente inexplorada en el contexto de los biocompuestos PLA/CNCs es su polimorfismo cristalino (Dhar et al., 2015). La celulosa nativa (tipo I) presenta cadenas con una configuración paralela y compactamente empaquetadas, con una red densa de puentes de hidrógeno intra e intermoleculares que confieren alta rigidez y baja accesibilidad química (Duchemin, 2015). La celulosa II, en cambio, se obtiene mediante mercerización con tratamientos alcalinos con NaOH a concentraciones superiores al 12–18% p/v o regeneración en solución, y adopta una configuración antiparalela de cadenas termodinámicamente más estable, con un patrón de enlaces de hidrógeno diferente y una red cristalina más abierta(Carrillo-Varela et al., 2018; Zlenko et al., 2021).

Este reordenamiento estructural tiene implicaciones directas sobre la reactividad química y la eficiencia de la hidrólisis ácida. La disposición antiparalela y el mayor volumen libre de la celulosa II generan una mayor densidad de grupos

hidroxilo superficiales expuestos y accesibles, lo que puede facilitar tanto la hidrólisis ácida como las reacciones de modificación superficial posteriores (Nagarajan et al., 2017). Sin embargo, la literatura reporta resultados contradictorios sobre las propiedades de los CNCs de tipo II en comparación con los de tipo I, y escasean los estudios que comparen sistemáticamente ambos polimorfos en el contexto de su incorporación en biocompuestos de PLA (Dhar et al., 2015; Wu et al., 2018; Zhao et al., 2016). Esta brecha limita el uso estratégico del polimorfo más adecuado para aplicaciones específicas de alto rendimiento.

I.5. MODIFICACIÓN SUPERFICIAL DE LOS CNCS

El principal obstáculo para la compatibilización de los CNCs con matrices hidrofóbicas como el PLA es su carácter intrínsecamente hidrofílico, originado producto de la elevada densidad de grupos hidroxilo libres en la superficie y en los grupos éster sulfato introducidos durante la hidrólisis con ácido sulfúrico (Bangar et al., 2022). La incompatibilidad interfacial resulta en aglomeración severa de las nanopartículas, reducción de la interfase para la transferencia de esfuerzos y degradación de las propiedades mecánicas del nanocompuesto (Dufresne, 2019; Sukmawan et al., 2023). Entre las estrategias de modificación superficial exploradas se encuentran esterificación, sililación, carboximetilación y oxidación TEMPO, no obstante, la acetilación con anhídrido acético ha demostrado ser una de las más eficientes para incrementar la hidrofobicidad de los CNCs manteniendo su integridad cristalina (Ávila Ramírez et al., 2017; Gan et al., 2017).

La acetilación introduce grupos acetilo (–$OCOCH_3$) en sustitución de los grupos hidroxilo superficiales, reduciendo la polaridad de la superficie y favoreciendo la dispersión de los CNCs en solventes orgánicos y en matrices poliméricas apolares (Lin et al., 2011; Spinella et al., 2015). El grado de sustitución (DS), puede varía entre 0 y 3 en función de la accesibilidad de los grupos –OH disponibles, es el parámetro clave para cuantificar la extensión de la modificación y controlar el balance hidrofílico-hidrofóbico de los nanorefuerzos (Gan et al., 2017; Li et al., 2024). Estudios previos han reportado que la acetilación superficial de CNCs en matrices PLA produce mejoras moderadas a significativas en las propiedades

mecánicas, térmicas y de barrera de los biocompuestos resultantes, aunque la magnitud de estos efectos varía de acuerdo con el DS alcanzado, procesamiento del material y del estado de dispersión de las partículas en la matriz (Agustin et al., 2016; Lee et al., 2020; Spinella et al., 2015).

I.6. BIOCOMPUESTOS PLA/CNCS, AVANCES Y BRECHAS

La literatura sobre biocompuestos PLA/CNCs ha ido creciendo exponencialmente en la última década (Ryoo et al., 2025). Estudios demostraron que la incorporación de CNCs en matrices de PLA puede aumentar el módulo de Young, la temperatura de degradación y la cristalinidad de la matriz, particularmente cuando se utilizan CNCs modificados superficialmente o compatibilizadores (Eichers et al., 2022; Fortunati et al., 2012; Trivedi & Gupta, 2024). Sin embargo, la mayoría de estos trabajos se han centrado exclusivamente en CNCs de celulosa tipo I provenientes de algodón o microcristalina comercial, dejando una brecha considerable en el conocimiento sobre el comportamiento de los CNCs de tipo II como nanorefuerzos y agentes nucleantes en matrices de PLA (Dhar et al., 2015).

Asimismo, a pesar de los avances en la acetilación de CNCs de tipo I, el impacto del polimorfismo sobre la eficiencia de la reacción de acetilación que suele ser expresada como DS y sobre las propiedades de los biocompuestos resultantes no ha sido sistemáticamente caracterizado (Chen et al., 2023; Wu et al., 2018; Zhao et al., 2016). La hipótesis de que la arquitectura molecular de la celulosa II debido a su mayor accesibilidad química podría conducir a un DS superior mediante condiciones de reacción idénticas, y que este mayor DS se traduciría en una compatibilidad interfacial mejorada y mejores propiedades del biocompuesto, no se ha puesto en práctica experimentalmente hasta el presente trabajo. Esta investigación responde precisamente a dicha brecha del conocimiento, utilizando como materia prima un valioso recurso forestal de Chile, la pulpa Kraft de eucalipto, contribuyendo así a la valorización de la cadena productiva forestal nacional mediante el desarrollo de materiales avanzados de embalaje sostenible.

II. HIPÓTESIS

"La estructura polimórfica de los nanocristales de celulosa influye directamente en la eficiencia de la acetilación superficial. Bajo las mismas condiciones de reacción, los nanocristales de celulosa II presentarán un mayor grado de sustitución que los nanocristales de celulosa I, debido a la mayor accesibilidad química derivada de su disposición antiparalela de cadenas. Como consecuencia, al ser incorporados en una matriz de PLA, los nanocristales de celulosa II acetilados conferirán al material biocompuesto una mayor cristalinidad de la matriz, estabilidad térmica y propiedades mecánicas superiores a las obtenidas con nanocristales de celulosa I acetilados"

III. OBJETIVOS

III.1. OBJETIVO GENERAL

Producir y comparar nanocristales de celulosa de los polimorfos I y II, derivados de pulpa Kraft de eucalipto en sus formas no modificada y acetilada, e incorporarlos como nanorefuerzos en películas biocompuestas de ácido poliláctico (PLA), para determinar la influencia del polimorfismo celulósico y la modificación superficial sobre las propiedades fisicoquímicas, estructurales, térmicas y mecánicas del material resultante

III.2. OBJETIVOS ESPECÍFICOS

1. Obtener y caracterizar nanocristales de celulosa de polimorfos I y II (CNC I y CNC II) a partir de pulpa Kraft blanqueada de eucalipto mediante hidrólisis con ácido sulfúrico, y determinar el efecto de la acetilación heterogénea con anhídrido acético sobre la morfología, química superficial y estructura cristalina de los nanocristales, cuantificando el grado de sustitución (DS) y los cambios en contenido de azufre y potencial Zeta.
2. Fabricar películas biocompuestas de PLA nanoreforzadas con CNC I, CNC II, ACNC I y ACNC II a concentraciones de 0,5; 1,0 y 1,5% en masa, y evaluar el tipo de nanorefuerzo y su concentración sobre la cristalinidad de la matriz

de PLA mediante difracción de rayos X (XRD) y calorimetría diferencial de barrido (DSC), identificando la formulación con mayor capacidad nucleante.

3. Determinar el efecto del tipo de nanorefuerzo y su concentración sobre la estabilidad térmica y las propiedades mecánicas de las películas biocompuestas, estableciendo un rango de carga óptimo en términos del balance de los resultados.

IV. ARTÍCULO CIENTÍFICO

El siguiente manuscrito corresponde al artículo científico sometido a la revista *Cellulose*. Se presentan todas las secciones del artículo incluyendo; Introducción, materiales y métodos, resultados, discusión y conclusiones propias del artículo de acuerdo con el formato estándar de la revista indicada.

Acetylated cellulose I and II nanocrystals from eucalyptus kraft pulp as nucleating nanofillers for poly(lactic acid) biocomposites

Cristóbal Donoso[1,2], Isidora Reyes-Gonzalez[1,2],David Guarda[1,2], María Graciela Aguayo[3,4], Fabiola Valdebenito[5],María S. Peresin[6,7], Regis Teixeira Mendonça[1,2,8,*]

[1]Facultad de Ciencias Forestales, Universidad de Concepción, Concepción, Chile.
[2]Laboratorio de Biopolímeros y Materiales Biobasados, Centro de Biotecnología, Universidad de Concepción, Concepción, Chile.
[3]Departamento de Ingeniería en Maderas, Universidad del Bío-Bío, Concepción 4081112, Chile.
[4]Centro de Biomateriales y Nanotecnología, Universidad del Bío-Bío, Concepción 4081112, Chile.
[5]Centro de Energía, Universidad Católica de la Santísima Concepción, Concepción 4090541, Chile.
[6]Sustainable Bio-Based Materials Laboratory, College of Forestry and Wildlife Sciences, Auburn University, Auburn, AL, 36849, USA
[7]Wood Utilization + Design Institute, Clemson University, 321 Harris A. Smith Building, Clemson, SC 29631, USA.
[8]Centro de Innovación en Tecnología y Diseño de Materiales para el Entorno Construido—CIMAC-ANID CTI250005, Santiago 9170022, Chile.

*Corresponding author: RT Mendonça (rteixeira@udec.cl)

INTRODUCTION

Over the years, there has been growing concern about the environmental impact of pollution from petrochemical plastics and synthetic materials. This has driven a global search for innovative, sustainable, and degradable biomaterials, particularly within the packaging sector, where the massive generation of plastic waste demands solutions that align with the principles of a circular economy (Melchor-Martínez et al., 2022; Omran et al., 2021). In this context, biomaterials derived from renewable resources that possess the ability to biodegrade present themselves as a highly promising alternative (Agbakoba et al., 2023).

The production of sustainable biomaterials has focused on various biopolymers, with polylactic acid (PLA) being one of the most prominent (Wi et al., 2025). Thanks to its renewable origin and complete biodegradability, PLA has positioned itself as a leading material for development across multiple industries. However, its widespread application is hindered by several drawbacks (Dhar et al., 2017). Its amorphous and semi-crystalline forms vary significantly depending on the processing method, and its intrinsically slow crystallization rate delays industrial processing and limits its mechanical properties (Nofar et al., 2019; Vatansever et al., 2019). Characteristics such as brittleness and low ductility restrict the application of pure PLA in sectors that require high-performance, robust packaging (Shin et al., 2022).

To overcome these limitations, the incorporation of nanofillers, specifically cellulose nanocrystals (CNCs), has gained significant attention. CNCs are highly crystalline rod-like nanostructures, typically 5–50 nm in width and 100–500 nm in length, derived from cellulose while retaining the crystalline framework of their biological source (Peng et al., 2021). These rod-like nanoreinforcements are notable for their low density, high stiffness, thermal stability, and biodegradability, making them ideal candidates for improving the thermomechanical properties of a wide range of materials (Mariano et al., 2014; Rashid et al., 2023). A key structural feature of cellulose is its polymorphism. Native cellulose (type I) has a parallel chain configuration, making it highly compact and rigid (Carrillo-Varela et al., 2018). In contrast, cellulose II is a thermodynamically more stable form obtained through

regeneration or mercerization, and it exhibits an antiparallel chain arrangement (Duchemin, 2015; Zlenko et al., 2021). Understanding these polymorphic differences is fundamental, as their distinct crystalline structures significantly impact the chemical accessibility and final properties of the nanoreinforced biocomposites (Carrillo-Varela et al., 2024; Gil-Castell et al., 2022).

The inherent characteristics of CNCs, including their high surface to volume ratio and abundance of surface hydroxyl groups, make them ideal candidates for targeted chemical modification (Dufresne, 2019; Rana et al., 2021). Typically, the extraction process via sulfuric acid hydrolysis introduces sulfate groups onto the CNC surface (López et al., 2025; Ma et al., 2021). While these groups provide colloidal stability, they also impart a highly hydrophilic character, resulting in poor compatibility with hydrophobic matrices (Bangar et al., 2022; Sukmawan et al., 2023). One effective strategy to improve their performance is to introduce hydrophobic surface modifications, such as acetylation (Ávila Ramírez et al., 2017; Gan et al., 2017; Sun et al., 2021). This replaces polar hydroxyl groups with hydrophobic acetyl groups, significantly improving the compatibility and dispersion of CNCs within hydrophobic polymer matrices, specifically PLA (Bayat et al., 2025; Ryoo et al., 2025). This modification strengthens interfacial interactions, prevents severe agglomeration, and ultimately enhances the mechanical and barrier properties of the resulting nanocomposites (Eichers et al., 2022; Lim et al., 2025).

Despite these advances in the surface modification of cellulose nanocrystals, most research has focused exclusively on type I derived nanostructures (Dong et al., 2017). This leaves a significant gap in our knowledge regarding the systematic comparison of type I and type II polymorphs (Dhar et al., 2015). In cellulose II, the antiparallel chain arrangement and the stacking of glucopyranose rings along the (1–10) plane generate a higher density of exposed surface hydroxyl groups, which drastically increases its hydrophilicity and propensity for severe particle agglomeration via hydrogen bonding (Dong et al., 2017; Espino-Pérez et al., 2013; Nagarajan et al., 2017). The altered hydrogen bond network and increased hydroxyl density may significantly enhance chemical accessibility during acetylation reactions. This structural advantage could potentially yield a higher degree of

substitution, thereby improving interfacial compatibility with hydrophobic polymer matrices (Chen et al., 2023; Yoo & Youngblood, 2016). However, there is a lack of comprehensive studies comparing the acetylation efficiency, thermal stability, and nucleating capacity of CNC I versus CNC II within PLA biocomposites. This knowledge gap limits the strategic selection of optimal cellulose polymorphs for targeted applications (Zhao et al., 2016). Furthermore, a deeper understanding of how polymorphic structure influences interfacial interactions between acetylated nanoreinforcements and the PLA matrix is necessary for designing high-performance, sustainable materials with enhanced mechanical and thermal properties (Wu et al., 2018).

Therefore, this study focuses on developing PLA nanocomposites reinforced with CNCs derived from both polymorphs I and II, evaluating them in both their unmodified and acetylated forms. It is hypothesized that the altered molecular architecture of CNC II will facilitate a higher degree of acetylation compared to CNC I under identical reaction conditions, potentially leading to superior interfacial interaction with the PLA matrix. This enhanced compatibility is expected to result in improved mechanical properties, including tensile strength, elongation, and stiffness, as well as increased thermal stability. The results of this research are expected to provide fundamental insights for the rational design of CNC nanoreinforced biomaterials, expanding their potential for sustainable packaging and other high-performance applications.

MATERIALS AND METHODS

Materials

Polylactic acid (PLA, Ingeo™ Biopolymer 4043D, NatureWorks LLC, Minnetonka, MN, USA) was used as the polymer matrix. It was processed without further purification or drying beyond the manufacturer's storage recommendations. The cellulose starting material was bleached eucalyptus kraft pulp (80% Eucalyptus nitens and 20% E. globulus), kindly donated by CMPC S.A. Chemical solutions and treatments were prepared using deionized water produced by a Barnstead D4741 nanopure deionization system (Barnstead/Thermolyne Corp., Dubuque, IA, USA).

The main chemicals used in this work were sodium hydroxide lentils (≥ 99%), pyridine (≥ 99%), acetic acid (≥ 99.7%), and acetic anhydride (≥ 99%), all obtained from Sigma-Aldrich. Sulfuric acid (95–97% p.a., EMSURE ISO) and dichloromethane (≥ 99.8%, stabilized) were purchased from VWR Chemicals BDH (Avantor Sciences).

Alkalization Treatments

Alkaline extraction was performed using cellulose pulp hydrated to a consistency of 10% (m/v). This process was based on the modified methodology described by Reyes-González et al. (2024). The main objectives of this step were to eliminate residual hemicellulosic components and to reorganize the cellulose chains. The sodium hydroxide solutions used were NaOH at 7% (m/v) to obtain cellulose I and NaOH at 20% (m/v) for conversion to cellulose II. The reaction was carried out for 1 h at 30 °C, after which the pulp was washed and filtered to remove excess reagents and water until a neutral pH was reached, resulting in a consistency of 30–35% (m/v). The obtained cellulose I and cellulose II pulps were stored for producing cellulose nanocrystals I and II.

Preparation of Cellulose Nanocrystals

The CNCs were produced through a four-step process involving acid hydrolysis, washing, dialysis, and ultrasonication. This methodology followed the procedure described by Gil-Castell et al. (2022). Initially, the cellulose pulp was subjected to acid hydrolysis using a solution of 55% sulfuric acid (H_2SO_4) at a pulp-to-acid ratio of 1:40. The reaction was stirred constantly for 45 min at a controlled temperature of 60 °C. Following hydrolysis, the reaction was quenched by dilution with excess distilled water and then neutralized. The resulting mixture was washed three times by centrifugation at 10,000 rpm for 10 min per cycle to remove any residual acid. The precipitate was then placed in a dialysis bag with a 12 kDa membrane and immersed in distilled water. The water was changed frequently until a neutral pH was achieved. Finally, the neutralized suspension underwent ultrasonic treatment in a cold-water bath at 750 W for 10 min using pulsed cycles. The

suspension was then centrifuged under the same conditions as previously. The concentrated CNC suspension obtained was stored in a desiccator at room temperature and served as the base material for subsequent characterization and acetylation procedures.

Acetylation of Cellulose Nanocrystals

The CNCs were chemically modified through a heterogeneous phase acetylation reaction using previously freeze-dried material, following a methodology adapted from Chen et al. (2023); Rahimi Kord Sofla et al. (2019). First, the CNCs were dispersed in a mixture of 50 ml of pyridine and 15 ml of acetic acid. The resulting suspension was subjected to bath sonication in a cold bath for 20 min. The mixture was then sealed in a flask and heated to 50 °C. Then, 75 ml of acetic anhydride and 0.1 ml of sulfuric acid were added, and the reaction was stirred constantly at 50 °C for 3 h. Acetone was then added to stop the reaction, and the acetylated product was separated via centrifugation. The suspension was repeatedly centrifuged, first with acetone to ensure the complete removal of residual reagents and then with distilled water until a neutral pH was achieved. Finally, the ACNC I and ACNC II samples were freeze-dried and stored for use in PLA biocomposite films.

Preparation of Biocomposites Films PLA/CNCs

The biocomposite films were fabricated using the solvent casting method with a total mass of 1 g. Thirteen samples were prepared, as detailed in Table 1. For this process, PLA was dissolved in 20 ml of dichloromethane (DCM) under constant stirring for 1 h. Meanwhile, the CNCs were dispersed in an additional 20 ml of DCM and subjected to sonication at 25% amplitude for 2 min, a step repeated twice. Then, both solutions were mixed under constant agitation for 10 min. The mixture was sonicated again under the previously mentioned conditions to achieve uniform dispersion of the nanoreinforcements in the PLA matrix. Next, the mixture was poured into Petri dishes, and the casting process was carried out at 25 °C for 24 h under controlled temperature and humidity conditions to ensure uniform solvent evaporation. The resulting films were stored for subsequent characterization.

Table 1. Treatments and factor levels of the 4x3 factorial design plus control.

Treatment	Nanoreinforcement type	CNCs content (%)
1	CNC I	0.5
2	CNC I	1
3	CNC I	1.5
4	CNC II	0.5
5	CNC II	1
6	CNC II	1.5
7	ACNC I	0.5
8	ACNC I	1
9	ACNC I	1.5
10	ACNC II	0.5
11	ACNC II	1
12	ACNC II	1.5
13	Control (Neat PLA)	0

Characterization of Cellulose Nanocrystals

Transmission Electron Microscopy (TEM)

The morphology and dimensions of the CNCs and ACNCs were analyzed using a JEM-1200 EX II transmission electron microscope (JEOL Ltd., Tokyo, Japan) operated at an acceleration voltage of 100 kV. To prepare the samples, a diluted suspension of CNCs and ACNCs (0.5 wt%) was sonicated for 10 min to ensure optimal dispersion. Then, a 5 µL aliquot of the suspension was deposited on carbon-coated copper grids (300 mesh) and left to dry at room temperature. Bright-field images were obtained at different magnifications using 50 and 100 nm scale bars to visualize the individual cellulose nanocrystals and observe their characteristic morphology.

Elemental Analyses

The sulfur content of CNCs and ACNCs was determined by elemental analysis using an elemental analyzer (Elementar vario MICRO, Ronkonkoma, NY, USA). Samples were analyzed in triplicate to determine the total sulfur (S) content of each nanocrystal type. The average values, reported as mg of sulfur per gram of

nanocrystal, were used to evaluate the effect of acetylation and cellulose polymorphism on surface chemistry.

Zeta Potential

The colloidal stability of CNC and ACNC samples was evaluated by measuring their zeta potential (ζ). Measurements were performed in triplicate at room temperature using a Litesizer 500 (Anton Paar, Austria). The surface charge of the cellulose nanocrystals was analyzed in diluted aqueous suspensions (0.5 wt%), after sonication for 10 min at 25% amplitude. These values were used to evaluate the impact of cellulose polymorphism and acetylation on the electrostatic stabilization of the suspensions.

Degree of substitution (DS)

The DS of the acetylated CNCs (ACNC I and ACNC II) was determined using a modified heterogeneous saponification back-titration method based on the procedure reported by Duan et al. (2022). For the analysis, 100 mg of freeze-dried ACNC I and ACNC II samples were weighed. The samples were sonicated for 4 min at 25% amplitude in 50 ml of distilled water. Then, 25 ml of NaOH 0.25 M were added, and the solution was stirred for 30 min. The excess unconsumed NaOH was then titrated with a standard HCl 0.5 M solution until a neutral pH was obtained. Blank solutions without ACNC samples were titrated using the same procedure for comparison. The DS was calculated using the following expression (1):

$$(1)\ DS = (162 \times (V_1 - V_2) \times C)/(42 \times m - 42 \times (V_1 - V_2) \times C)$$

C is the concentration of the standard HCl solution (0.5 M); V_1 and V_2 are the volumes of HCl (ml) consumed by the blank solution and the ACNCs samples, respectively; m is the mass of the ACNCs (g); 162 corresponds to the molar mass of the glucoside units (g/mol); and 42 is the molar mass of the acetyl group minus one hydrogen atom (g/mol) (Duan et al., 2022).

Fourier Transform Infrared (FTIR)

The chemical composition of CNC and ACNC samples was analyzed by Fourier transform infrared spectroscopy (FTIR). Spectra were recorded in the range of 4000–500 cm^{-1} at room temperature using a PerkinElmer Spectrum 400 FTIR system (PerkinElmer, USA). Each spectrum was recorded for a total of 64 scans with a resolution of 4 cm^{-1}.

X-Ray Diffraction (XRD)

The crystallographic parameters of CNCs were determined by X-ray diffraction (XRD) analysis. Instrumental measurements were performed using a Rigaku SmartLab SE diffractometer with Bragg-Brentano geometry, employing Cu Kα radiation (λ = 1.541 Å) at 40 kV and 50 mA. The samples were analyzed in triplicate within the 2θ angular range of 5° to 50°, at a step size of 0.01° and a scanning speed of 10°/min.

Quantitative phase analysis and unit cell refinement were performed using the Rietveld method implemented in the software MAUD (Materials Analysis Using Diffraction, version 2.9993, University of Trento, Italy). Structural models for cellulose I and cellulose II were taken from crystallographic information files (CIF) retrieved from the Crystallography Open Database (COD), corresponding to the crystal structures reported by Langan et al. (2001) for cellulose I and by Kaduk and Blanton (2013) for structural model of cellulose II. An amorphous contribution was included in all refinements as an additional phase to account for the non-crystalline fraction of the samples, allowing the software to discriminate between the crystalline and amorphous components of the diffraction pattern.

Refinement was carried out following a sequential fitting strategy in which parameters were progressively introduced and refined in the following order: background, zero-shift, scale factor, unit cell parameters (lattice lengths a, b, c and γ angle), and crystallite size for the crystalline phase, using the specific CIF corresponding to cellulose I or cellulose II depending on the sample. Atomic positions were kept fixed at the values reported in the reference CIF structures throughout the refinement, to preserve the physical consistency of the structural

model and avoid overparameterization. The background was modelled using a polynomial function, and peak profiles were fitted with a pseudo-Voigt function (French, 2021). The quality of each refinement was evaluated using the weighted profile residual (Rwp), accepting only refinements with Rwp values below 10% as statistically reliable. The apparent crystallinity index (CI) of each sample was calculated as the ratio between the refined crystalline phase fraction and the total diffracted intensity, while the refined unit cell parameters (a, b, c and γ) were used to assess lattice distortions associated with acid hydrolysis and the processing conditions applied during CNC extraction.

Characterization of Biocomposites Films PLA/CNCs

X-Ray Diffraction (XRD)

The crystallographic parameters of biocomposites films PLA/CNCs were determined by X-ray diffraction (XRD) analysis. Instrumental measurements were performed using a Rigaku SmartLab SE diffractometer with Bragg-Brentano geometry, employing Cu Kα radiation (λ = 1.541 Å) at 40 kV and 50 mA. The samples were analyzed in triplicate within the 2θ angular range of 5° to 50°, at a step size of 0.01° and a scanning speed of 10°/min.

To evaluate the crystalline nature of the nanomaterials, the diffraction patterns were fitted, and the baseline was subtracted by interpolation to perform background correction using the software PeakFit V4.12 (Systat Software, San José, CA). The peak deconvolution method was then applied to the diffractograms, assuming that a broad Gaussian band represented the amorphous contribution to the total broadening. Curve fitting was performed using Gaussian models, and the quality of the fit was validated by a F-number greater than 45,000 ($R^2 > 0.997$) in all cases. Finally, the apparent crystallinity index (CI) of the samples was calculated using the following equation (2):

$$(2)\ \mathrm{CI}\ (\%) = A_{Cryst}/A_{Total} \times 100$$

Where A_{Cryst} is the sum of the crystalline areas and A_{Total} is the total area provided by the diffractogram (Carrillo-Varela et al., 2018; Park et al., 2010). The lateral crystal size (L) was then calculated using the following equation (3):

$$(3)\ L = (k \times \lambda)/(\beta \times \cos\theta)$$

Where L is the lateral crystal size (nm), k is Scherrer's constant (0.96), λ is the X-ray wavelength, β is the full width at half maximum (FWHM), and θ is the Bragg reflection corresponding to the (200) plane of cellulose (Carrillo-Varela et al., 2018; Scherrer, 1918).

Film Thickness

The thickness of the biocomposite films was measured using a D-2000 digital micrometer (Electromatic Equipment Co., Inc., USA) equipped with two flat, parallel circular pressure surfaces, in accordance with ISO 534:2005. For each formulation, at least three measurements were taken at different positions of the film, and the average value was used as the representative thickness. Before mechanical testing, the thickness of every individual tensile specimen was measured and entered the RSA 3 instrument software to ensure accurate calculation of tensile strength, elongation, and Young's modulus based on the actual cross-sectional area of each sample.

Mechanical Testing

The tensile properties of the biocomposite films (tensile strength, elongation, and Young's modulus) were determined according to ASTM D882 (Standard Test Method for Tensile Properties of Thin Plastic Sheeting). A static uniaxial tensile test was carried out using an RSA 3 dynamic mechanical analyzer (TA Instruments, New Castle, DE, USA). Rectangular strips were cut from the films with their long axis aligned with the casting direction. The initial gauge length, cross-head speed, and specimen width were set following the ASTM D882 recommendations; the previously measured thickness values were introduced into the instrument software to calculate

the engineering stress and modulus parameters. At least four specimens were tested for each formulation, and the results are reported as the mean ± standard deviation.

Fourier Transform Infrared (FTIR)

The chemical structure of the biocomposite films was analyzed by Fourier transform infrared (FTIR) spectroscopy. Spectra were recorded at room temperature in the range 4000–500 cm^{-1} using a PerkinElmer Spectrum 400 FTIR spectrometer (PerkinElmer, USA). For each sample, 64 scans were collected at a resolution of 4 cm^{-1} and averaged to obtain the final spectrum.

Thermogravimetric Analysis (TGA)

Thermogravimetric analysis of the biocomposite films was performed using a Q500 thermogravimetric analyzer (TA Instruments, New Castle, DE, USA). Samples with masses between 6 and 8 mg were placed in platinum pans and heated from 25 °C to 650 °C at a heating rate of 10 °C/min under a nitrogen atmosphere (flow rate 60 mL/min). The onset and maximum degradation temperatures, as well as the residual mass at 650 °C, were obtained from the TGA and derivative thermogravimetric (DTG) curves.

Differential Scanning Calorimetry (DSC)

Differential scanning calorimetry was carried out using a PerkinElmer STA 6000 instrument (PerkinElmer, USA) in accordance with ASTM D3418. Film samples of approximately 10 mg were sealed in aluminum pans; an empty pan was used as reference. The specimens were heated from 30 to 300 °C at a constant rate of 10 °C/min under a nitrogen atmosphere. From the DSC thermograms, the glass transition temperature (Tg), the cold crystallization temperature (Tcc) and enthalpy (ΔHcc), and the melting temperature (Tm) and enthalpy (ΔHm) of the PLA matrix were determined. The degree of crystallinity of PLA in each biocomposite (Xc) was calculated using (4):

$$(4)\ \mathrm{Xc} = (\Delta\mathrm{Hm} - \Delta\mathrm{Hcc})/(\Delta\mathrm{H°m} \times \mathrm{Wpla})$$

Where ΔHm is the melting enthalpy of the biocomposite film, ΔHcc is the cold-crystallization enthalpy, ΔH°m is the melting enthalpy of 100% crystalline PLA reported in the literature (93 J/g), and Wpla is the mass fraction of PLA in the biocomposite (Sullivan et al., 2015).

Design of experiment

The influence of formulation variables on the properties of the biocomposites was studied using a 4 × 3 factorial designs. Two independent factors were considered: (i) nanoreinforcement type, with four levels (CNC I, CNC II, ACNC I, and ACNC II), and (ii) cellulose nanocrystal loading, with three levels (0.5, 1.0, and 1.5 wt%). This design yielded 12 nanoreinforced biocomposites, plus a neat PLA film used as control, for a total of 13 treatments (Table 1).

Structural (XRD), thermal (DSC, TGA), and mechanical (tensile) response variables were analyzed mainly by two-way analysis of variance (ANOVA), considering nanoreinforcement type and loading as fixed factors and adopting a 95% confidence level ($p < 0.05$). When the two-way ANOVA indicated significant main effects or interactions, Tukey's honestly significant difference (HSD) post hoc test was applied to identify differences between specific factor levels or formulations. In addition, for selected XRD variables, one-way ANOVA followed by Tukey's HSD was used to compare all individual formulations with the neat PLA film considered as a reference group. The results are expressed as mean ± standard deviation. All statistical analyses were performed using OriginPro version 9 (OriginLab Corporation, Northampton, MA, USA), and the results are expressed as mean ± standard deviation.

RESULTS AND DISCUSSION

Characterization of Cellulose Nanocrystals

Transmission Electron Microscopy (TEM)

TEM analysis revealed marked morphological transformations throughout the processing sequence of the cellulose nanocrystals. Aqueous suspensions of CNC I

and CNC II, analyzed immediately after sulfuric acid hydrolysis and before freeze-drying, exhibited the expected rod-like morphology of cellulose nanocrystals, with individualized particles clearly distinguishable in both samples (Figure 1a, b). CNC I presented well-dispersed, needle-shaped particles with dimensions typical of sulfuric-acid-hydrolyzed CNCs, whereas CNC II displayed similar rod-like structures but with slightly more variable dimensions, a behavior commonly associated with the different chain packing and accessibility of the cellulose II allomorph compared with cellulose I (Gong et al., 2017). Both suspensions showed good separation of individual particles in their aqueous state, confirming the successful extraction of cellulose nanocrystals from both polymorphs by sulfuric acid hydrolysis.

However, the freeze-drying step induced drastic morphological changes in both CNC I and CNC II (Figure 1c, d). Water sublimation during lyophilization led to severe aggregation, completely altering the original rod-like morphology. In both cases, the dried samples transformed into dense, irregular, almost spherical aggregates with ill-defined boundaries and characteristic length scales on the order of tens of nanometers, and the original fibrillar structure of the cellulose nanocrystals was no longer evident. These consolidated aggregates are formed through the establishment of multiple intermolecular hydrogen bonds between adjacent nanocrystal surfaces as water is removed, a phenomenon widely described as hornification in cellulose-rich systems. Similar spheroidal or compact aggregated morphologies have been reported for CNCs and related cellulosic nanoparticles after freeze-drying or solvent-exchange drying, where initially individualized rods self-assemble into dense particles or foams driven by van der Waals forces and extensive hydrogen bonding, with suspension concentration and surface charge density governing the transition from discrete nanocrystals to aggregated domains (Abdallah & Kamal, 2018). Recent work by Huntington et al. (2023) further supports that drying-induced hornification corresponds to a kinetically trapped state in which reswelling and redispersion are strongly hindered by non-covalent bonding network formed upon drying.

Following acetylation, ACNC I and ACNC II exhibited massive and persistent aggregation (Figure 1e, f), essentially identical to that observed in their lyophilized

CNC precursors. Despite the partial substitution of surface hydroxyl groups by acetyl moieties confirmed by FTIR and elemental analysis, the acetylation reaction did not reverse the hornification-induced aggregation. Both acetylated samples displayed irregular, dense agglomerates and did not recover the original individualized rod-like morphology. These observations suggest that the chemical modification predominantly occurred on the external surfaces and more accessible regions of the aggregates and did not penetrate deeply enough to disrupt the compact hydrogen-bonded core and separate the nanocrystals. The intra and intermolecular hydrogen bonds generated during lyophilization thus appear to persist even after superficial acetylation, indicating that once hornification occurs under these processing conditions, redispersion of CNCs into their initial rod-like state is extremely difficult and may require alternative drying or redispersion strategies, such as solvent exchange, additives, or high-energy mechanical processing (Al Hakkak et al., 2019).

These morphological changes have direct implications for interpreting the performance of the processed biocomposites. The aggregated state of the lyophilized cellulose nanocrystals substantially reduces their effective specific surface area available for interfacial interactions with the PLA matrix. This morphological constraint helps explain the modest improvements in mechanical properties observed during tensile testing, despite the outstanding increases in matrix crystallinity and thermal stability achieved in the PLA biocomposite films. In other words, while ACNC II acted as a highly efficient nucleating agent at the matrix scale, the persistent aggregation of the nanocrystals likely limited stress transfer across the interface, constraining the potential reinforcement effect.

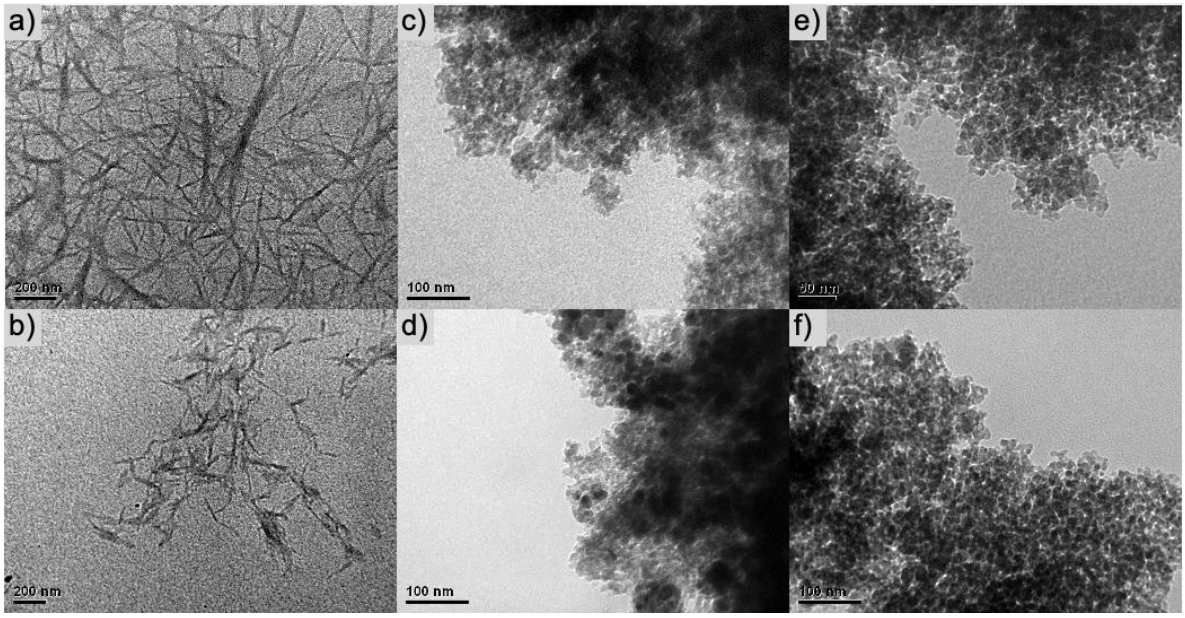

Figure 1. Transmission electron microscopy (TEM) images of 0.5 wt% cellulose nanocrystals suspensions showing the morphological evolution through processing stages a) CNC I fresh aqueous suspension after acid hydrolysis b) CNC II fresh aqueous suspension after acid hydrolysis c) freeze-dried CNC I d) freeze-dried CNC II e) ACNC I after acetylation f) ACNC II after acetylation.

Fourier Transform Infrared (FTIR)

Both CNC I and CNC II exhibit the fundamental absorption bands characteristic of cellulose, as shown in Figure 2. A prominent, broad band in the 3200–3500 cm^{-1} region is attributed to the stretching vibrations of O–H bonds within the extensive hydrogen-bond network of cellulose, consistent with the typical O–H stretching band reported around 3400 cm^{-1} for native and regenerated cellulose. Additionally, the C–H asymmetric stretching vibration is observed in the 2900–2937 cm^{-1} range, corresponding to the aliphatic C–H stretching of the glucopyranose ring and pendant groups, in agreement with previous FTIR studies of cellulose nanocrystals and related cellulosic substrates (Reyes-González et al., 2024). A comparative inspection of the spectra reveals that the absorbance intensities of both the O–H band (3440–3450 cm^{-1}) and the C–H band (2900–2937 cm^{-1}) are higher for the type II polymorph than for the type I polymorph (Figure 2). This difference can

be associated with the distinct supramolecular organization of cellulose II generated by mercerization, in which the original intramolecular hydrogen bonds of cellulose I are disrupted and the chains reorganize into an antiparallel arrangement with a modified hydrogen-bonding network and altered free-volume distribution, leading to a larger fraction of spectroscopically accessible O–H and C–H groups (Gong et al., 2017; Wang et al., 2022).

After acetylation, the formation of ester groups in ACNC I and ACNC II is evidenced by the appearance of a sharp, intense carbonyl (C=O) stretching band at approximately 1745 cm^{-1}, which provides direct proof of the substitution of surface hydroxyl groups by acetyl moieties and is consistent with the ester carbonyl band reported for acetylated cellulose nanocrystals. In addition, a new absorption band emerges in the 1230–1250 cm^{-1} region, assigned to the C–O stretching vibration of the ester linkage, in agreement with previous FTIR studies of acetylated nanocellulose (Oberlintner et al., 2023). Despite the strong presence of these ester bands, the broad O–H stretching signal remains clearly detectable in both acetylated samples, indicating that a significant fraction of hydroxyl groups is still present. This persistence of the O–H band suggests that acetylation was predominantly confined to the more accessible surface regions of the nanocrystals and the outer zones of the aggregates, while the inner crystalline domains retained their native cellulose backbone and hydrogen-bonding framework, as commonly observed for heterogeneous surface acetylation of CNCs. These findings are fully consistent with the moderate degree of substitution determined for ACNC I and the higher, yet still partial, substitution obtained for ACNC II described on the follow sections (2017; Li et al., 2019; Yu et al., 2021; Zlenko et al., 2021).

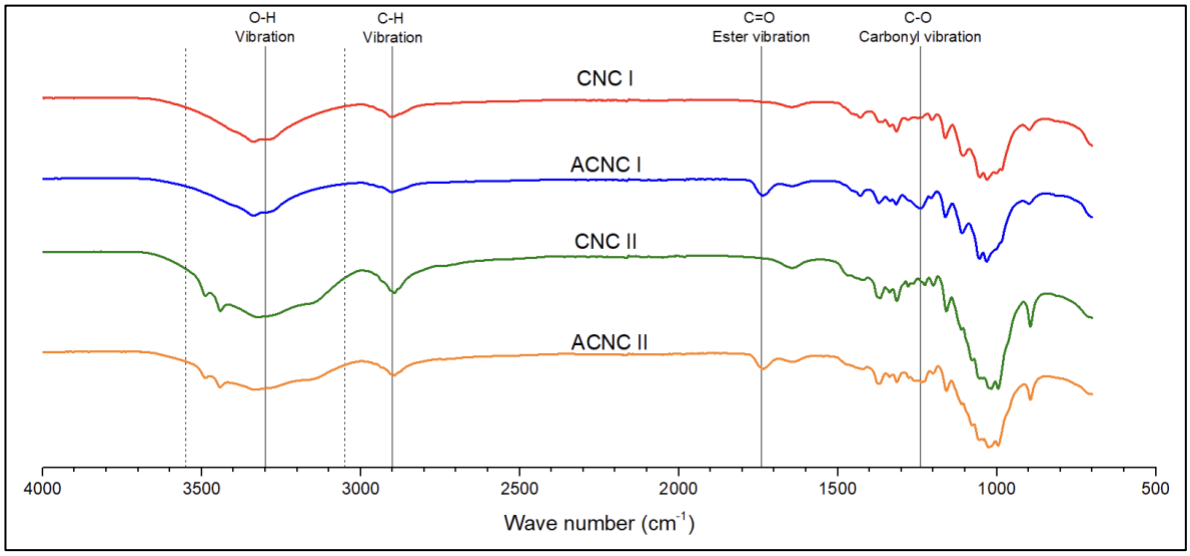

Figure 2. FTIR spectra of cellulose nanocrystals (CNC I and CNC II) and their respective acetylated derivatives (ACNC I and ACNC II) recorded in the 4000–500 cm⁻¹ region, highlighting the O–H and C–H stretching bands and the ester C=O and C–O vibrations introduced by acetylation.

Zeta Potential and Sulfur Content

The results for surface sulfur content and zeta potential for the four cellulose nanocrystal variants are summarized in Table 2. These parameters provide insight into the surface chemistry, colloidal stability, and expected thermal behavior of the nanostructures prior to their incorporation into the PLA matrix.

The sulfur content reflects the density of sulfate ester groups ($–OSO_3^-$) grafted onto the CNC surface during sulfuric acid hydrolysis. CNC I exhibited the highest sulfur content (4.63 ± 0.59 mg/g), which is consistent with the relatively compact and highly ordered structure of the cellulose I polymorph obtained from kraft pulp under the selected hydrolysis conditions. In contrast, CNC II presented a substantially lower sulfur content (1.97 ± 0.56 mg/g). This decrease suggests that the mercerized cellulose II structure, with its antiparallel chain arrangement and modified accessibility, is more susceptible to acid-induced degradation and partial dissolution of surface chains under identical hydrolysis conditions, leaving fewer sulfate half-ester groups attached to the remaining crystallites. These results indicate

that cellulose polymorphism directly influences hydrolysis efficiency and the resulting surface functionalization of the cellulose nanocrystals (Ferro et al., 2020).

Acetylation caused a further reduction in sulfur content for both ACNC I and ACNC II, to 1.02 ± 0.16 and 1.39 ± 0.07 mg/g, respectively (Table 2). This decrease shows that the acetylation reaction carried out in pyridine with acetic anhydride and acetic acid promoted partial desulfation of the CNC surfaces, in agreement with reports where post-treatments or surface functionalization reduce the amount of sulfate groups and improve thermal performance. This side effect is beneficial for the intended high-temperature processing of PLA nanocomposites, because sulfate ester groups are known to catalyze the thermal degradation of cellulose and shift the onset of decomposition to lower temperatures (Lam et al., 2022). Therefore, the partial removal of sulfate groups during acetylation is expected to contribute to the enhanced thermal stability observed for the acetylated nanocrystals and their corresponding PLA biocomposites, as discussed in the characterization of biocomposites PLA/CNCs section (López et al., 2025).

The zeta potential values reflect the electrostatic repulsion in the electrical double layer surrounding the particles and, therefore, the colloidal stability of the aqueous suspensions. All samples showed negative zeta potentials in a narrow range between -22.3 and -24.4 mV (Table 2). These magnitudes are comparable to those reported by Aguayo et al. (2020) for sulfuric acid derived CNCs from eucalyptus kraft pulp, which displayed moderately high negative zeta potentials and stable aqueous dispersions under similar conditions. The most negative values (-24.0 and -24.4 mV) corresponded to the hydrophilic precursors CNC I and CNC II, respectively, and are consistent with their higher sulfate group contents, which generate sufficient surface charge density upon dissociation in water to maintain colloidal stability and limit spontaneous aggregation. Interestingly, despite its lower total sulfur content, CNC II exhibited a zeta potential similar to that of CNC I, suggesting that in the cellulose II polymorph the remaining charged groups are in more exposed surface regions and thus contribute efficiently to the effective surface charge.

Following chemical modification, the acetylated samples (ACNC I and ACNC II) displayed slightly less negative zeta potentials of -22.3 and -22.7 mV, respectively. This modest decrease is consistent with the partial desulfation evidenced by the sulfur content data and the incorporation of electrically neutral acetyl groups, which together reduce the overall surface charge density (Jordan et al., 2019). Nevertheless, the values remain within the range typically associated with kinetically stable CNC suspensions, close to the commonly cited stability threshold of approximately -25 mV for electrostatically stabilized colloids. In this system, the combined effect of decreased surface charge and increased hydrophobicity is expected to favor compatibility with organic solvents and with the hydrophobic PLA matrix, while still providing sufficient electrostatic repulsion during the aqueous processing steps to avoid irreversible flocculation of the nanocrystals.

Table 2. Sulfur content and zeta potential values for cellulose nanocrystals (CNC I and CNC II) and their respective acetylated derivatives (ACNC I and ACNC II).

	Sulfur Content (mg/g)	φz (mV)
CNC I	4.63 ± 0.59	-24.0 ± 0.6
ACNC I	1.02 ± 0.16	-22.3 ± 0.6
CNC II	1.97 ± 0.56	-24.4 ± 0.6
ACNC II	1.39 ± 0.07	-22.7 ± 1.1

Degree of Substitution (DS)

The degree of substitution (DS) was used to quantify the chemical acetylation of the cellulose nanocrystals. The DS represents the average number of hydroxyl groups replaced by acetyl groups per anhydroglucose unit (AGU), with a theoretical maximum value of 3 for fully substituted cellulose. The experimental values obtained for the acetylated samples are summarized in Table 3 and compared graphically in Figure 3.

Under identical acetylation conditions, the reactivity of the cellulose I and cellulose II polymorphs differed markedly. The ACNC I sample reached a DS of 0.23 ± 0.07, which corresponds to a relatively low substitution level typically associated

with predominantly surface-confined esterification; in this case, the highly compact crystalline packing and rigid hydrogen-bond network characteristic of the CNC I structure limit the diffusion of acetylation reagents into the crystal interior, so that esterification mainly occurs at the accessible hydroxyl groups located on the outer surfaces of the nanocrystals. In contrast, the ACNC II sample exhibited a much higher reaction efficiency, achieving a DS of 1.38 ± 0.15, approximately a six-fold increase in substitution capacity with respect to the type I polymorph (1.38 versus 0.23). This behavior can be attributed to the regenerated cellulose II structure, which displays a less compact crystalline lattice and an altered hydrogen-bonding pattern compared with native cellulose I, leading to larger free volume and higher accessibility of hydroxyl groups; these structural features facilitate the penetration of acetic anhydride and the associated catalysts not only to the external surface but also into subsurface regions of the type II nanocrystals, enabling more extensive acetylation throughout a larger fraction of the crystalline domains (Dong et al., 2017).

The DS value of 1.38 achieved for ACNC II is comparatively high when contrasted with previously reported acetylation results for cellulose nanocrystal polymorphs. For example, Chen et al. (2023) reported DS values of 1.68 for ACNC I and 1.12 for ACNC III in a heterogeneous acetic-anhydride system, showing that CNC I can reach a high degree of substitution. Wu et al. (2018) observed a stronger contrast between polymorphs, with ACNC I attained a DS of 1.98 while ACNC II only reached a value of 0.32 after 3 h of acetylation in a similar heterogeneous medium. Additionally, (Dong et al., 2017) prepared ACNC II by a single-step phosphoric-acid/ acetic-anhydride method and obtained DS values between about 0.6 and 1.6 depending on reaction temperature. In this system, the sixfold increase in DS for cellulose type II compared to cellulose type I (1.38 versus 0.23) under identical reaction conditions (acetic anhydride, pyridine and acetic acid at 50 °C for 3 h) therefore reveals an opposite trend to that observed by Wu et al. (2018) and underscores that the regenerated cellulose II used here provides high chemical accessibility during acetylation, likely due to its specific combination of free volume, aggregation state and antiparallel chain packing.

As the DS increases, fewer free hydrophilic hydroxyl groups remain exposed in the cellulose nanocrystal structure, which leads to a progressive reduction in surface polarity. This trend is consistent with studies in which controlled acetylation of CNCs has been used to adjust the DS over a wide range and thereby modulate surface polarity and potential applications in different matrices. In the case of ACNC II, the DS of 1.38 is consistent with the pronounced decrease in the intensity of the O–H stretching band and the appearance of characteristic ester carbonyl and C–O stretching bands in the FTIR spectra, confirming the successful incorporation of acetyl groups. Under the same reaction conditions, the high reactivity of the cellulose II polymorph therefore establishes ACNC II as a more suitable nanoreinforcement than ACNC I when a high DS and enhanced hydrophobicity are required, and it is expected to display superior interfacial affinity with the PLA matrix during biocomposite film processing (Li et al., 2024).

It is important to note that the back-titration method used to determine the degree of substitution provides a bulk, average value and cannot distinguish between highly substituted regions on a limited, more accessible fraction of the material and a more uniform, moderate substitution throughout the entire particle population. In view of the extensive aggregation observed for freeze-dried cellulose nanocrystals by TEM, the DS values reported here should therefore be regarded as effective, apparent degrees of substitution that mainly reflect the more accessible surface regions of the CNC aggregates. This interpretation is consistent with the FTIR results, where the intensity of the acetyl-related bands confirms surface acetylation but does not necessarily imply homogeneous substitution of all internal crystalline domains.

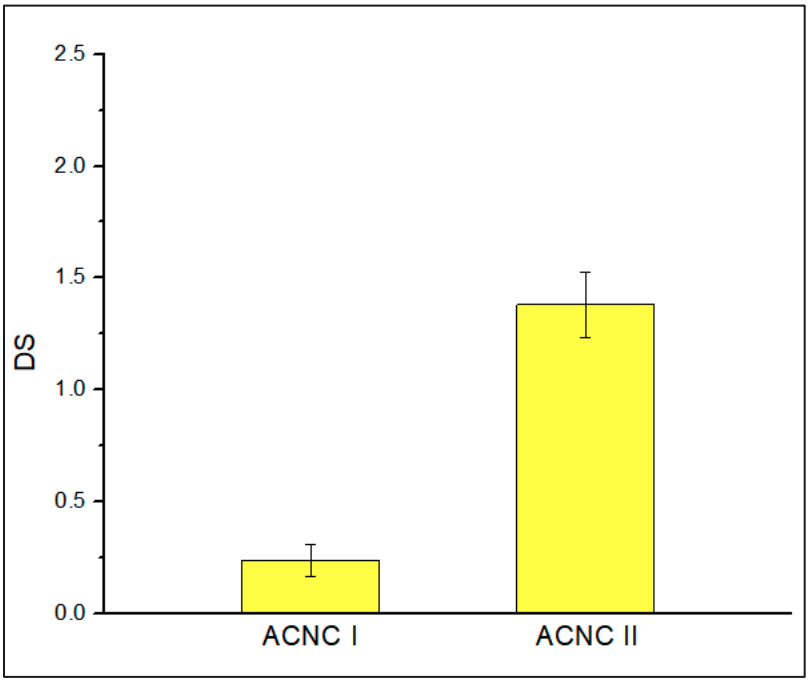

Figure 3. Graphical representation of the DS for the ACNC I and ACNC II nanoreinforcements.

Table 3. Experimental DS values for the acetylated cellulose nanocrystals (ACNC I and ACNC II).

Sample	Degree of substitution
ACNC I	0.23 ± 0.07
ACNC II	1.38 ± 0.15

X-Ray Diffraction (XRD)

XRD analysis was employed to identify changes in the polymorphic structure of the cellulose nanocrystals and to evaluate the impact of chemical acetylation on their crystallinity and unit cell geometry. The diffraction patterns and the corresponding structural parameters are presented in Figure 4 and Table 4, respectively.

The diffractograms clearly evidence the structural transition between the two polymorphs. CNC I and ACNC I display characteristic reflections at approximately 2θ = 14.7°, 16.5°, and 22.6°, which can be indexed to the (110), (1–10), and (200) crystallographic planes of cellulose I, respectively. These peaks confirm that the

native cellulose I framework is fully preserved after sulfuric-acid hydrolysis and subsequent acetylation. In contrast, the patterns of CNC II and ACNC II show distinctive peaks at 2θ ≈ 12.1°, 20.0°, and 22.0°, corresponding to the (1–10), (110), and (020) planes of cellulose II, respectively, together with an additional reflection at around 34.5° that can be assigned to the (040) plane, which appears in both polymorphs. These crystallographic fingerprints are consistent with earlier reports that characterized the polymorphic shift from cellulose I to cellulose II in alkalized eucalyptus fibers (Carrillo-Varela et al., 2018).

The crystallinity index (CI) obtained through Rietveld refinement for the present samples is in reasonable agreement with the ranges previously reported for CNCs from bleached kraft pulp and for cellulose II-based nanocrystals. For sulfuric-acid-derived CNCs from eucalyptus kraft pulp, Aguayo et al. (2020) described CI values between 66 and 82%, which closely match the 67.00 % obtained here for CNC I. For cellulose II nanocrystals extracted from Potenza et al. (2022) reported CI values of approximately 63–75%, confirming that the crystallinity obtained for CNC II (66.64 %) falls within the expected range for this polymorph.

Following chemical modification, the samples exhibited an overall high degree of crystallinity retention, with opposite trends between polymorphs. For the type I polymorph, a slight decrease in crystallinity is observed, from 67.00 ± 3.15% in CNC I to 65.28 ± 2.31% in ACNC I. This minor loss can be ascribed to the substitution of surface hydroxyl groups by bulkier acetyl moieties, which introduces a limited degree of structural disorder at the crystal boundaries. Conversely, a more pronounced increase in crystallinity was recorded for the type II polymorph, from 66.64 ± 2.95% in CNC II to 70.74 ± 3.00% in ACNC II. This behavior may indicate that acetylation of cellulose II preferentially affects the more disordered domains rather than the crystalline core, and partial removal or rearrangement of residual amorphous regions could lead to an apparent increase in crystallinity without implying true growth of the crystalline domains.

This trend contrasts with results reported by Chen et al. (2023), where surface acetylation of sulfuric-acid-hydrolyzed CNC I resulted in a noticeable decrease in crystallinity, indicating partial surface erosion or disordering of the nanocrystal

structure upon extensive acetylation. In our case, the preservation and slight enhancement of crystallinity in ACNC II may be related to the lower initial crystallinity of the CNC II precursor compared with CNC I, as a larger amorphous fraction offers more material available for selective degradation or reorganization during acetylation without compromising the crystalline core (Gan et al., 2017; Xu et al., 2020).

Regarding the unit cell parameters, the values reported in Table 4 provide further insight into the structural response of each polymorph to acetylation. For CNC I, the refined lattice parameters are broadly consistent with the monoclinic unit cell reported for the Iβ allomorph of native cellulose, which is typically described with γ close to 96–97°, reflecting the characteristic sheet-like packing of cellulose chains (Nishiyama et al., 2002). After acetylation, ACNC I show a contraction along the c-axis accompanied by a slight increase in the a-axis and in γ, suggesting a modest distortion of the unit cell associated with the incorporation of acetyl substituents at the crystal surface, consistent with the minor crystallinity loss discussed above.

For the cellulose II polymorph, the CNC II unit cell shows a markedly larger γ angle than cellulose I, in agreement with the antiparallel chain packing that characterizes the cellulose II monoclinic lattice, typically reported with γ in the range of 117–120° (Langan et al., 2001). After acetylation, ACNC II exhibits a contraction in the a-axis and a corresponding decrease in γ, together with a narrower dispersion in the b-axis, suggesting a more compact and structurally homogeneous unit cell. This tightening of the lattice geometry is consistent with the increase in crystallinity observed for ACNC II, supporting the interpretation that acetylation promoted a reorganization of the crystalline lattice toward a more ordered configuration rather than degrading the crystalline core.

Overall, the combination of crystallinity and unit cell data confirms that the acetylation treatment, although structurally more impactful for cellulose II in terms of degree of substitution, did not compromise the crystalline integrity of either polymorph. This preservation of the crystalline architecture, together with the moderate lattice adjustments observed after acetylation, is value to support the use of these cellulose nanocrystals as reinforcing and nucleating agents in polymer matrices, particularly cellulose II-based nanocrystals, whose lattice compaction upon

acetylation may translate into improved interfacial compatibility with hydrophobic matrices such as PLA.

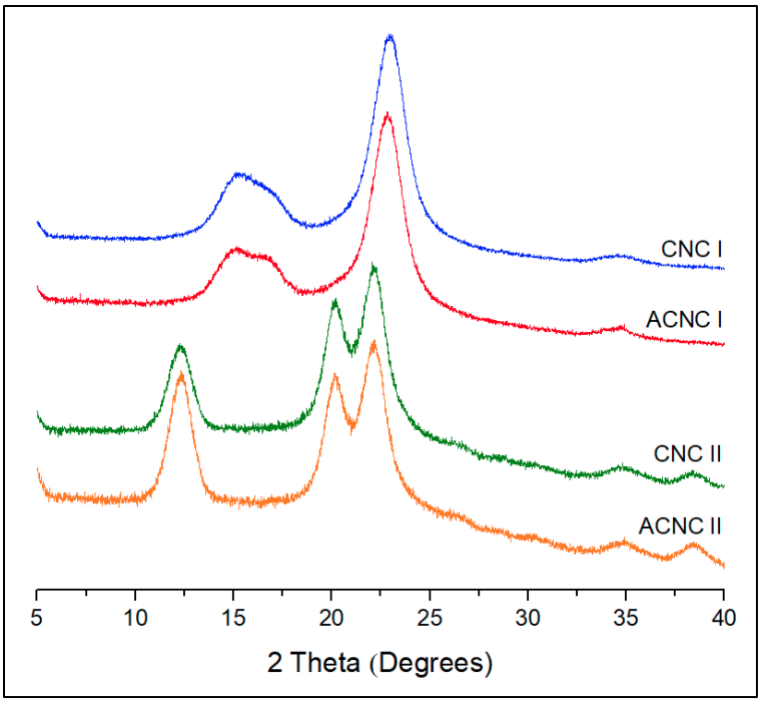

Figure 4. XRD patterns of cellulose nanocrystals (CNC I and CNC II) and their respective acetylated derivates (ACNC I and ACNC II).

Table 4. Apparent crystallinity index (%) and unit cell parameters (a, b, c, and γ) of CNC I, ACNC I, CNC II, and ACNC II, determined by Rietveld refinement of the XRD data.

	CI	Length a	Length b	Length c	Length γ
	(%)		(Å)		(°)
CNC I	67.00 ± 3.15	7.34 ± 0.45	7.00 ± 0.86	8.48 ± 1.93	96.16 ± 0.27
ACNC I	65.28 ± 2.31	7.66 ± 0.29	7.02 ± 0.78	6.73 ± 0.36	98.49 ± 2.63
CNC II	66.64 ± 2.95	8.34 ± 0.53	9.27 ± 0.39	8.07 ± 1.11	119.77 ± 1.17
ACNC II	70.74 ± 3.00	7.35 ± 0.21	8.57 ± 0.09	7.92 ± 0.96	116.66 ± 0.40

Characterization of Biocomposites PLA/CNCs

X-Ray Diffraction (XRD)

X-ray diffraction was used to evaluate the influence of cellulose nanocrystals on the molecular organization of the polylactic acid matrix. The diffraction patterns

of the biocomposite films are shown in Figure 5, and Table 5 summarizes the crystallinity indices (CI) calculated for both the PLA phase and the dispersed nanoreinforcements within each formulation.

A two-way ANOVA performed on the PLA phase CI revealed highly significant effects of nanoreinforcement type ($p = 1.48 \times 10^{-24}$) and concentration ($p = 3.71 \times 10^{-6}$), as well as a significant interaction ($p = 1.76 \times 10^{-2}$), indicating that the crystallization response of PLA is strongly controlled by both the structural nature and the loading level of the nanocrystals.

In the diffractograms (Figure 5a,b), all biocomposites exhibit the broad amorphous halo of PLA centered at approximately $2\theta \approx 16.5°$, corresponding to the overlapping (110)/(200) reflections of α-PLA. Additional weak peaks at around 12.5°, 18.5°, and 32.0° can be assigned to the (010), (203), and (118) planes of the α polymorph, respectively, which are characteristic of semicrystalline PLA. Although the individual diffraction signals of the cellulose nanocrystals are not clearly resolved in the films due to the relatively low filler contents and the predominance of the PLA halo, their presence is indirectly reflected in the changes of PLA crystallinity and in the CI values assigned to the dispersed CNCs, obtained by peak deconvolution.

Tukey's HSD test, applied to the PLA CI across all formulations, showed that neat PLA (13.32 %) does not differ significantly from any CNC I formulation at 0.5, 1.0, or 1.5 wt% ($p = 0.56$, 0.88, and 0.65, respectively), indicating that CNC I have a limited ability to act as nucleating agents under the present solvent-casting conditions. By contrast, all PLA/CNC II formulations at 0.5, 1.0, or 1.5 wt% exhibit PLA CI values significantly higher than neat PLA ($p = 1.40 \times 10^{-3}$, $p = 1.49 \times 10^{-5}$ and $p = 2.40 \times 10^{-7}$, respectively), confirming that CNC II provide more effective heterogeneous nucleation sites than cellulose I even in their unmodified state. These observations agree with previous reports in which modest, but consistent, increases in PLA crystallinity were attributed to the templating effect of rigid nanocellulose domains dispersed in the matrix (Trivedi & Gupta, 2024).

The nucleating capability of the cellulose nanocrystals is markedly enhanced upon acetylation. For both ACNC I and ACNC II, the PLA CI increases sharply even at the lowest loading (0.5 wt%), and all PLA/ACNC formulations differ significantly

from neat PLA. When the Type factor is analyzed as a main effect, ACNC II yields significantly higher PLA crystallinity than ACNC I ($p = 1.0 \times 10^{-4}$). These results clearly indicate that acetylation enhances the nucleating efficiency of cellulose nanocrystals in general, and that ACNC II is the most effective nucleating agent among the four types investigated.

At the concentration factor, PLA/ACNC II films consistently display the highest PLA CI values at each concentration, with PLA/ACNC II 1.5 wt% reaching 44.20 %, corresponding to more than a threefold increase relative to neat PLA. when averaged across all concentrations, its overall nucleating performance is superior. This superior behavior can be rationalized by the higher degree of substitution of ACNC II, its lower sulfate content, and the preservation of its crystalline structure, which together improve compatibility with PLA and facilitate more homogeneous dispersion, thereby increasing the number of effective nucleation sites during film formation.

The statistical analysis also provides insight into the saturation behavior of the system. Within each series, increasing the cellulose nanocrystals content from 1.0 to 1.5 wt% does not lead to significant changes in the PLA crystallinity index ($p = 0.99$ for CNC I, $p = 0.84$ for CNC II, $p = 0.80$ for ACNC I and $p = 0.74$ for ACNC II), suggesting that a near-saturation of available nucleation sites is reached at around 1.0 wt% for all types. Beyond this threshold, additional nanocrystals likely contribute less effectively to crystallization, possibly due to an increased tendency to form local aggregates that act as inactive or less efficient nucleating domains. Similar saturation effects have been reported in other PLA/nanocellulose systems, where increases in crystallinity on the order of 15–25% relative to neat PLA are typically observed at higher filler contents (≥ 3–5 wt%), especially when surfactant-modified or compatibilized CNCs are employed (Fortunati et al., 2012). More broadly, reviews of PLA-based biocomposites indicate that nanocellulose and other rigid fillers generally produce moderate crystallinity enhancements, whose magnitude depends strongly on filler chemistry, dispersion state and processing route, with only a limited number of systems reaching the upper range of improvements observed here. Although direct quantitative comparison is restricted

by differences in PLA grade, processing conditions and crystallinity determination methods, the present values therefore fall within the highest nucleation-driven crystallinity levels reported for PLA/nanocellulose biocomposites (Trivedi et al., 2023).

Overall, the XRD and statistical analyses demonstrate that cellulose nanocrystals are effective nucleating agents for PLA, with acetylated forms providing a clear enhancement of this function. Among all systems, ACNC II stand out as the best nucleating candidates, combining high intrinsic crystallinity, improved compatibility with PLA, and the ability to induce large increases in PLA crystallinity at relatively low loadings. These features position ACNC II as a particularly promising reinforcement for the design of PLA-based biocomposites with high crystallinity and potentially improved mechanical and thermal properties.

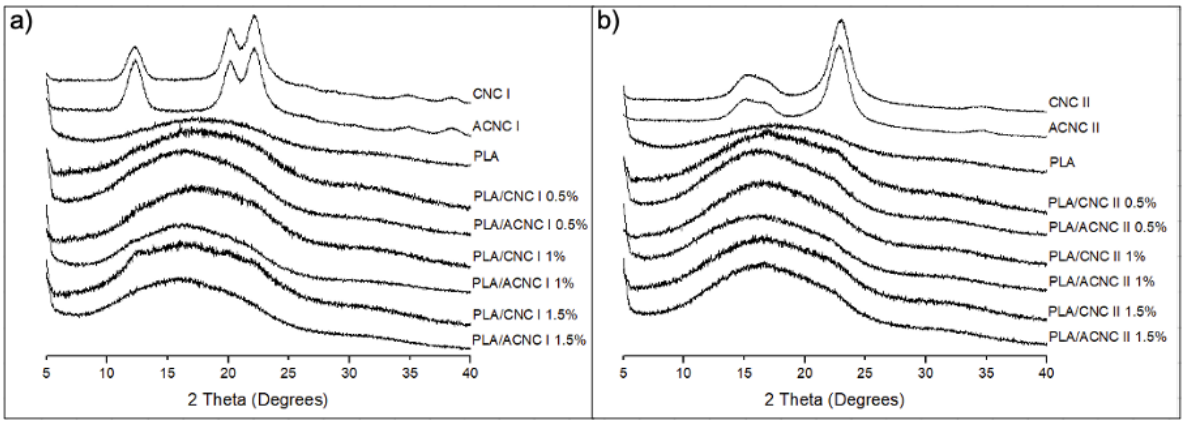

Figure 5. XRD patterns of biocomposite films a) formulations containing cellulose I nanocrystals (CNC I and ACNC I) and b) formulations containing cellulose II nanocrystals (CNC II and ACNC II). The diffraction patterns of neat PLA and powdered nanocrystals are included for reference.

Table 5. Crystallinity index (CI %) of the PLA matrix and the nanoreinforcements in the biocomposite films. Values are expressed as mean ± standard deviation (n = 3). An asterisk (*) in the PLA column indicates a value significantly different from neat PLA according to two-way ANOVA followed by Tukey's HSD test (p < 0.05).

	PLA	CNCs
	CI (%)	

PLA	13.32 ± 1.78	
PLA/CNC I 0.5	15.75 ±1.78	9.94 ± 1.00
PLA/CNC II 0.5	18.83 ±1.11 *	13.52 ±1.09
PLA/ACNC I 0.5	34.46 ±1.09 *	12.39 ± 0.82
PLA/ACNC II 0.5	38.27 ± 0.25 *	11.66 ± 0.5
PLA/CNC I 1.0	15.14 ± 0.75	13.36 ± 0.93
PLA/CNC II 1.0	20.78 ± 2.13 *	16.00 ± 0.93
PLA/ACNC I 1.0	36.56 ± 0.37 *	13.20 ± 0.86
PLA/ACNC II 1.0	42.08 ± 0.36 *	10.34 ± 0.49
PLA/CNC I 1.5	15.61 ± 0.62	13.14 ± 1.04
PLA/CNC II 1.5	22.68 ± 2.78 *	16.06 ± 3.04
PLA/ACNC I 1.5	38.57 ± 1.37 *	11.82 ± 0.99
PLA/ACNC II 1.5	44.20 ± 0.86 *	11.16 ± 5.78

Differential Scanning Calorimetry (DSC)

The DSC thermograms of the first heating scan of all films displayed a glass transition, a single endothermic melting peak, and no detectable cold crystallization exotherm (Figure 6.), confirming the semi-crystalline nature of the materials. The absence of a cold crystallization exotherm suggests that crystallization was largely completed during solvent casting, a behavior previously reported for casting solution PLA-based films (Mechernene et al., 2026).

The thermal parameters derived from the first heating scan are summarized in Table 6. The Tg of neat PLA (58.40 °C) showed a general tendency to increase in nanocomposite formulations, reaching up to 63.4 °C for PLA/ACNC I 1.5. This trend may reflect a reduction of free volume in the amorphous phase associated with the growing crystalline fraction, which could restrict segmental chain mobility. No plasticization effect was observed across any formulation, consistent with the hydrophobic character of both unmodified and acetylated CNCs.

The melting temperature (Tm) remained relatively stable across all samples, ranging between 149 and 151 °C (Table 6), suggesting that the crystalline structure of the PLA matrix was not substantially altered by the type or content of nanoreinforcement at the loadings studied. This observation is related with the XRD results discussed, where the diffraction patterns of all nanocomposite films retained

the characteristic peaks of the PLA, and supports the interpretation that CNC act primarily as nucleating agents rather than crystal structure modifiers (Dong et al., 2017; Fortunati et al., 2012; Sullivan et al., 2015).

The most pronounced effects of the nanocrystals are observed in the melting enthalpy (ΔHm) and the corresponding degree of crystallinity (Xc). Neat PLA exhibits an Xc of 27.33%, whereas all nanocomposite films show higher crystallinity values, with a clear trend of increasing Xc with CNC content, reaching up to 98.26% for PLA/CNC II 1.5 (Table 6). These large increases in Xc are fully consistent with the nucleating role of CNCs reported for both solution-cast and melt-processed PLA composites, and they closely mirror the higher CI obtained by XRD for the same formulations.

At equivalent loadings, CNC II consistently produce higher Xc values than CNC I. For instance, at 0.5 wt% loading, Xc reaches 93.85% for PLA/CNC II compared with 46.62% for PLA/CNC I, while at 1.5 wt% the values are 98.26% and 56.15%, respectively (Table 6). This behavior may be related to the distinct hydrogen-bonding topology and antiparallel chain arrangement of the cellulose II lattice, which could provide a more favorable interface for PLA chain adsorption and ordering than the parallel-chain arrangement of cellulose I. The higher Xc values obtained by DSC for PLA/CNC II films agree with the higher CI values determined by XRD for the same series, reinforcing the view that CNC II are intrinsically more efficient nucleating agents for PLA than CNC I.

Respecting to the effect of acetylation, PLA/ACNC I formulations tended to show higher Xc values compared to their unmodified PLA/CNC I counterparts at equivalent loadings, a trend that could be related to improved dispersion of ACNC I in the casting solvent, thereby increasing the effective nucleating surface area available to PLA chains during film formation. For ACNC II, acetylation appeared to have a less pronounced effect, particularly at low loadings where unmodified CNC II already promoted high degrees of crystallinity (Table 6).

Overall, the DSC results are in general agreement with the crystallinity trends observed by XRD, reinforcing the interpretation that CNC tend to promote PLA crystallization under solution casting conditions, with acetylation playing a secondary

but potentially relevant role in improving the dispersion and nucleating efficiency of cellulose I based nanocrystals.

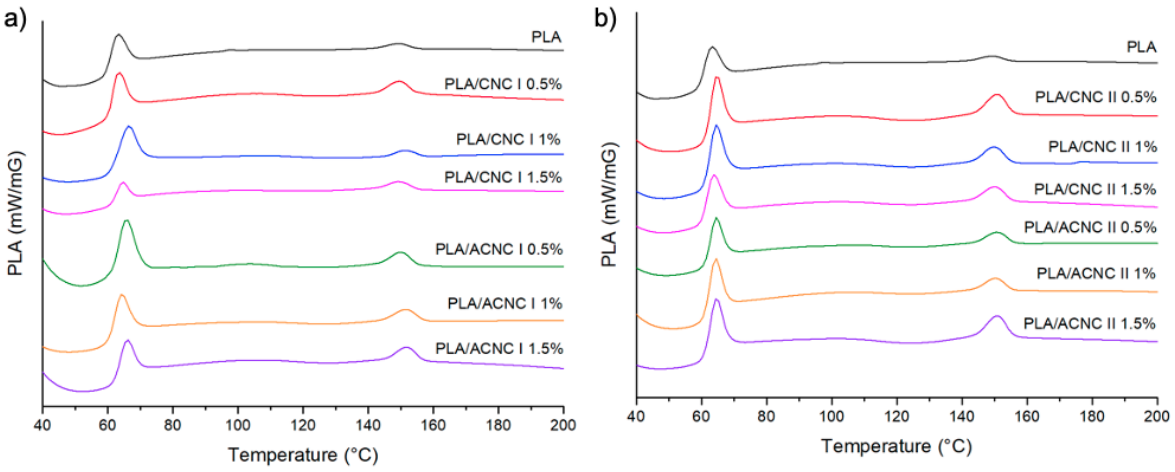

Figure 6. DSC thermograms (first heating scan) of neat PLA and PLA nanocomposite films a) PLA/CNC I and PLA/ACNC I b) PLA/CNC II and PLA/ACNC II. Curves are vertically offset for clarity.

Table 6. Glass transition temperature (Tg), melting temperature (Tm), melting enthalpy (ΔHm), and degree of crystallinity (Xc) of the PLA matrix and the nanoreinforcements in the biocomposite films obtained from DSC first heating scan.

	Tg	Tm	ΔHm	Xc
	(°C)		(J/g)	(%)
PLA	58.40	149.34	25.42	27.33
PLA/CNC I 0.5	58.70	149.90	43.14	46.62
PLA/ACNC I 0.5	60.26	150.26	49.43	53.42
PLA/CNC II 0.5	60.66	150.96	86.84	93.85
PLA/ACNC II 0.5	60.49	150.89	77.76	84.03
PLA/CNC I 1	59.34	151.43	45.13	49.02
PLA/ACNC I 1	61.82	151.11	70.57	76.65
PLA/CNC II 1	60.52	149.84	89.75	97.48
PLA/ACNC II 1	59.58	150.38	82.02	89.09
PLA/CNC I 1.5	60.89	149.50	51.44	56.15
PLA/ACNC I 1.5	63.37	151.27	72.08	78.68
PLA/CNC II 1.5	59.84	150.04	90.01	98.26

PLA/ACNC II 1.5	59.37	150.97	88.76	96.89

Thermogravimetric Analysis (TGA/DTG)

The thermal stability of the biocomposites was evaluated by thermogravimetric analysis and its first derivative. Figure 7 shows representative TGA and DTG curves for neat PLA and selected formulations (PLA/CNC I 1.5%, PLA/CNC II 1.5%, PLA/ACNC I 0.5%, PLA/ACNC II 0.5% and PLA/ACNC II 1.5%), whereas Table 7 summarizes the thermal degradation parameters ($T_{5\%}$, $T_{10\%}$, Tonset and Tmax) for all 13 formulations. These results indicate that the incorporation of cellulose nanocrystals modifies the degradation profile of the PLA matrix and that the magnitude of this effect depends on the surface chemistry and polymorphic structure of the nanoreinforcements.

According to the DTG curves, the neat PLA matrix exhibits an onset degradation temperature (Tonset) of 314.4 °C and a maximum degradation temperature (Tmax) of 344.3 °C (Table 7). After addition of nanoreinforcements, a general shift of the main degradation step towards higher temperatures is observed, particularly for formulations containing acetylated nanocrystals. For example, the PLA/ACNC II 1.5% sample shows a Tonset of 330.7 °C and a Tmax of 357.8 °C, increases of approximately 16 °C and more than 13 °C, respectively, compared with neat PLA. These improvements are consistent with the substantial increase in PLA crystallinity described in the XRD section, suggesting that the more ordered and compact crystalline regions formed in the presence of ACNCs act as physical barriers that restrict chain mobility and hinder the diffusion of volatile degradation products during heating.

Beyond this physical barrier effect, the enhanced stability of the PLA/ACNC biocomposites can be related to the chemical modification of the nanocrystals. Elemental analysis revealed a partial desulfation during acetylation, with sulfur contents decreasing from 4.63 to 1.02 mg/g for CNC I and ACNC I and from 1.97 to 1.39 mg/g for CNC II and ACNC II, respectively. Sulfate half-ester groups introduced during sulfuric acid hydrolysis are known to catalyze the thermal degradation of cellulose through acid-promoted depolymerization and dehydration reactions at

elevated temperatures. Their partial replacement by more thermally stable acetyl groups (–$OCOCH_3$) therefore reduces the number of catalytically active sites, which may contribute to the higher Tonset and Tmax values observed for the ACNC-based biocomposites. Similar trends, where removal or masking of sulfate groups leads to improved thermal stability of nanocellulose and its acetates, have been reported in previous studies (Kusmono et al., 2020).

Surface acetylation also increases the hydrophobic character of the nanocrystals, particularly for ACNC II, which reaches a degree of substitution of 1.38. This high substitution level markedly reduces the density of free hydroxyl groups on the nanocrystal surface and, consequently, its ability to absorb moisture. A lower moisture content in the reinforcement phase is expected to diminish hydrolytic contributions to degradation during heating and to favor stronger interfacial interactions with the hydrophobic PLA matrix. Such combined effects of improved compatibility and reduced moisture uptake on the thermal resistance of PLA/acetylated-CNCs systems are in line with previous reports, where enhancements in Tmax of about 8–15 °C have been described for similar nanocomposites (Agustin et al., 2016; Lee et al., 2020).

When analyzing the initial mass-loss temperatures ($T_{5\%}$ and $T_{10\%}$), most biocomposites display values comparable to or slightly higher than those of neat PLA, in agreement with the behavior of Tonset (Table 7). An exception is the PLA/ACNC II 1.0% sample, which exhibits an early mass loss at approximately 122 °C in $T_{5\%}$. Since this low-temperature event is not accompanied by a shift in the main degradation step and the subsequent Tonset and Tmax values remain similar to those of other ACNC II formulations, it is reasonable to attribute this mass loss to the release of residual solvent or moisture trapped in microcavities formed during the solvent-casting process, rather than to the onset of PLA degradation.

From a processing and formulation standpoint, the TGA results suggest that relatively low nanoreinforcement loadings are sufficient to obtain significant thermal stabilization. For instance, PLA/ACNC I 0.5% already reaches a Tmax of 353.9 °C, close to the highest value observed for PLA/ACNC II 1.5% (357.8 °C), and similar right-shifts of the DTG peak in Figure 7b. Together with the XRD and mechanical

results, which indicate a saturation of property improvements above 1.0 wt% nanocrystal content, these observations suggest that ACNC II loadings in the range 0.5–1.0 wt% constitute a promising compromise between enhanced thermal stability, mechanical performance and material efficiency, while also limiting the risk of particle agglomeration and processing defects at higher concentrations.

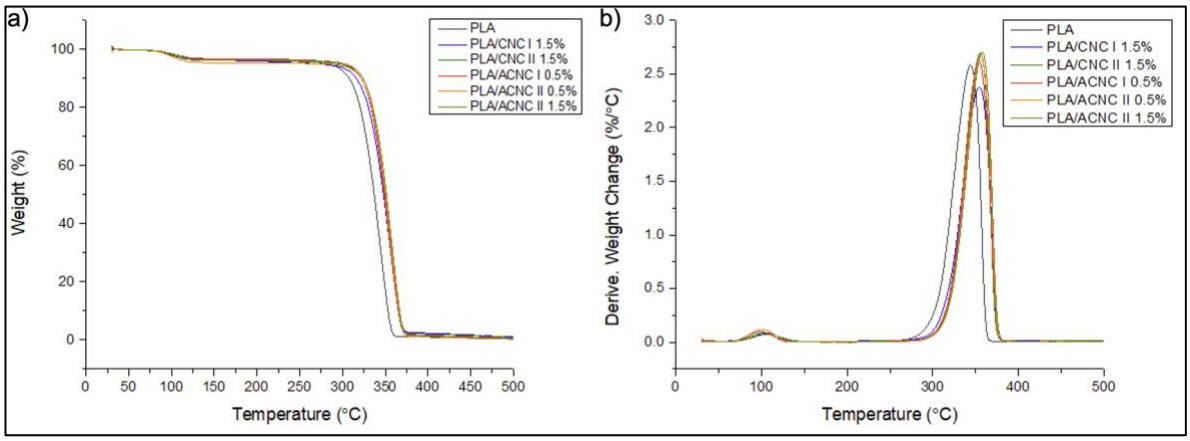

Figure 7. a) TGA curves of neat PLA and selected PLA-based nanocomposite films (PLA/CNC I 1.5%, PLA/CNC II 1.5%, PLA/ACNC I 0.5%, PLA/ACNC II 0.5% and PLA/ACNC II 1.5%) b) DTG curves highlighting the shift in maximum degradation temperature (Tmax) induced by the different nanoreinforcements. For clarity, only representative formulations are shown, complete thermal degradation parameters for all biocomposites are summarized in Table 7.

Table 7. TGA-derived thermal stability parameters for neat PLA and PLA/CNC biocomposite films, including temperatures at 5% and 10% mass loss ($T_{5\%}$, $T_{10\%}$), onset degradation temperature (Tonset), and temperature of maximum degradation rate (Tmax).

	Celsius degrees (°C)			
	$T_{5\%}$	$T_{10\%}$	Tonset	Tmax
CNC I	137.5	170.0	241.2	210.0
CNC II	119.0	158.1	249.0	219.0
PLA	282.1	307.7	314.4	344.3
PLA/CNC I 0.5	300.1	316.2	321.4	348.9
PLA/ACNC I 0.5	301.7	322	323.7	353.9

PLA/CNC II 0.5	305.8	320.6	326.1	350.1
PLA/ACNC II 0.5	269.3	321.8	324.5	356.3
PLA/CNC I 1	271.0	316.6	323.6	350.5
PLA/ACNC I 1	267.0	318.7	326.4	356.3
PLA/CNC II 1	297.1	317.8	327.4	345.8
PLA/ACNC II 1	122.0	318.6	328.6	356.3
PLA/CNC I 1.5	267.1	316.1	327.4	354.7
PLA/ACNC I 1.5	260.0	318.5	328	356.7
PLA/CNC II 1.5	294.3	321.7	330.4	355.6
PLA/ACNC II 1.5	302.4	324.0	330.7	357.8

Fourier Transform Infrared (FTIR)

Infrared spectroscopy of the biocomposite films was used to evaluate possible chemical interactions between the polylactic acid (PLA) matrix and the different cellulose nanocrystals (CNC I, ACNC I, CNC II and ACNC II). Figure 8 shows the FTIR spectra of the biocomposites together with those of neat PLA and the powdered nanoreinforcements.

The spectra are dominated by the vibrational bands of PLA, as expected from its high fraction in the formulations. All samples display the characteristic carbonyl stretching band (C=O) of PLA at 1747 cm^{-1}, the bending vibrations of methyl groups ($–CH_3$) near 1450 and 1360 cm^{-1}, and the C–O–C stretching region between 1180 and 1080 cm^{-1}, confirming that the chemical structure of the polyester backbone remains intact after solvent casting. This overall spectral profile agrees with typical FTIR signatures reported for PLA and PLA-based nanocomposite films (Yu et al., 2021).

A clear visual similarity is observed when comparing the FTIR spectrum of neat PLA with those of the biocomposites, which is consistent with the relatively low nanocrystal contents (0.5–1.5 wt%). The broad O–H stretching band associated with the surface hydroxyl groups of type I and type II cellulose appears with markedly reduced intensity in the PLA/CNC and PLA/ACNC films compared with the powdered nanocrystals. This reduction suggests that the hydroxyl groups of the nanocrystals are largely embedded in the PLA matrix and likely participate in weak intermolecular

interactions, such as hydrogen bonding with the carbonyl groups of the polyester, rather than remaining as a separate, highly hydrated phase. Increasing the nanoreinforcement loading from 0.5 to 1.5 wt% does not produce detectable shifts in the main PLA bands or the appearance of new peaks, indicating that the system behaves predominantly as a physical mixture without evidence of new covalent bond formation during processing. This behavior is consistent with previous PLA/CNC and PLA/cellulose nanofibril biocomposites, where FTIR changes are mainly reflected in band-intensity variations and broadening associated with hydrogen bonding rather than in new absorption bands (Wang et al., 2020).

In the biocomposite films containing ACNC I and ACNC II, the carbonyl absorption near 1750 cm^{-1} arises from the superposition of the ester groups of PLA and the acetyl groups grafted onto the nanocrystals. Although the individual contributions cannot be resolved due to peak overlap, the preservation of the band position and shape relative to the spectra of acetylated CNC powders supports the chemical stability of the acetyl functionalities within the PLA matrix. No systematic spectral differences are detected between films containing type I and type II polymorphs, which indicates that the overall chemical environment of the PLA chains and the nature of the interfacial interactions are similar for both polymorphs under the conditions studied. Consequently, the performance differences observed between CNC I/ACNC I and CNC II/ACNC II series are more likely governed by structural and morphological factors such as crystallization behavior, nucleating efficiency and dispersion quality rather than by distinct chemical bonding motifs at the interface.

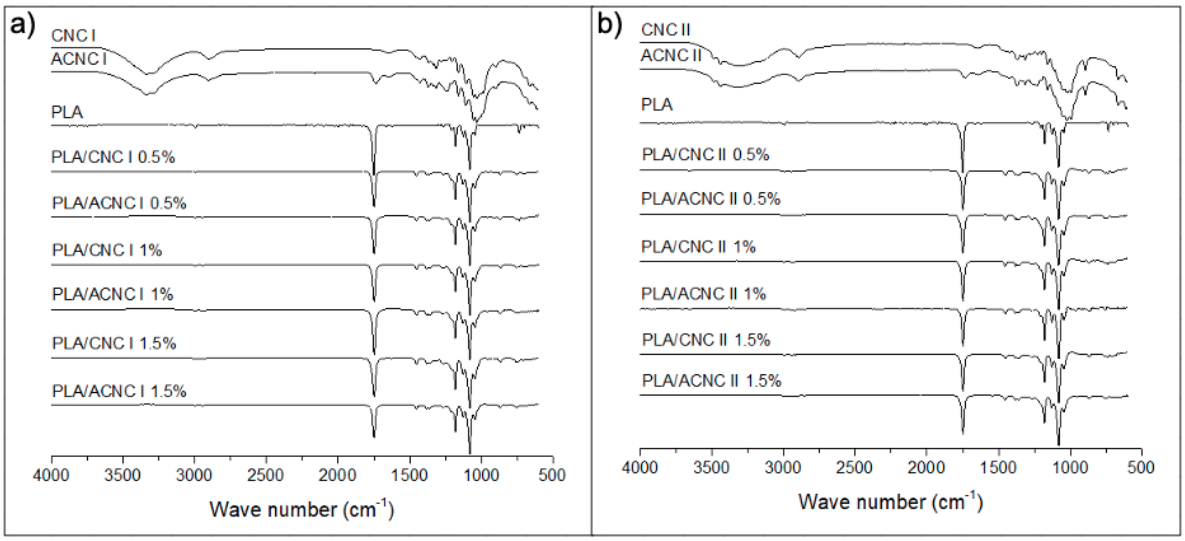

Figure 8. FTIR spectra of biocomposite films based on PLA and cellulose nanocrystals a) formulations containing cellulose I nanocrystals (CNC I and ACNC I) and b) formulations containing cellulose II nanocrystals (CNC II and ACNC II). The spectra of neat PLA and powdered nanocrystals are included for reference.

Mechanical Testing

The mechanical properties of the biocomposite films were evaluated through tensile testing to assess the influence of nanoreinforcement type and loading concentration on tensile strength, elongation, and Young's modulus. The results are summarized in Figure 9 and Table 8. A two-way ANOVA performed on tensile stress, elongation, and Young's modulus showed that neither the nanoreinforcement type nor its concentration, nor the interaction between both factors, produced statistically significant differences for any of the three mechanical parameters (tensile stress: $p = 0.259$ for type, $p = 0.219$ for concentration and $p = 0.708$ for the interaction; elongation: $p = 0.451$, 0.655 and 0.121; Young's modulus: $p = 0.123$, 0.351 and 0.257, respectively). Therefore, within the experimental conditions evaluated, no statistically supported mechanical improvement could be established for the PLA/CNC biocomposite films.

Overall, the incorporation of cellulose nanocrystals produces only modest changes in tensile stress, elongation and Young's modulus, with most values remaining within the scatter of the neat PLA reference. Although some formulations

show slightly higher tensile strength or modulus, the variability of the data and the relatively small sample size prevent these differences from being confirmed as statistically significant.

This lack of clear statistical evidence contrasts with the pronounced effects observed in the structural and thermal analyses, where XRD and DSC unequivocally demonstrated large increases in PLA crystallinity driven by the nanocrystals. In the present case, however, the combination of limited replicate number and relatively small increments in the mechanical parameters means that any potential reinforcement effect cannot be conclusively demonstrated and should be regarded primarily as indicative rather than definitive. Nevertheless, the results reveal a general tendency for the presence of cellulose nanocrystals to increase tensile stress, in many cases, elongation compared with neat PLA, particularly for films containing CNC II and ACNC II.

From a quantitative standpoint, the tensile strength (25.07–34.39 MPa), elongation (6.83–11.50%) and Young's modulus (265.40–438.17 MPa) measured for the solvent-cast PLA/CNC and PLA/ACNC films fall within the ranges commonly reported for PLA composites reinforced with cellulose nanocrystals or their surface-modified derivatives, where moderate increases in stiffness and only small changes in strength and ductility are typically observed. This agreement with the literature supports the view that, under the present processing conditions, CNCs and ACNCs act mainly as mild reinforcing agents that slightly stiffen the PLA matrix without imposing severe penalties on ductility, while the modest reinforcement observed here is plausibly limited by aggregation and hornification effects associated with freeze-drying of the nanocrystals. In the absence of direct fracture-surface imaging, this explanation should be regarded as a reasonable, literature-supported hypothesis rather than a quantitatively demonstrated mechanism (Bolat et al., 2024; Gong et al., 2017; Lee et al., 2020).

From a practical perspective, these findings indicate that the substantial crystallinity enhancements induced by CNCs under the selected processing conditions do not lead to a statistically detectable loss of tensile performance. On the contrary, the mechanical response of the nanocomposites remains comparable

to that of neat PLA, with some formulations exhibiting slight, non-significant improvements in strength and stiffness. Thus, the mechanical data support the view that CNC-based nanofillers can be used to tailor the crystalline structure and thermal behavior of PLA without detrimental effects on its basic tensile properties, even though a clear mechanical reinforcement could not be firmly established within the experimental uncertainty of this study (Nagarajan et al., 2015).

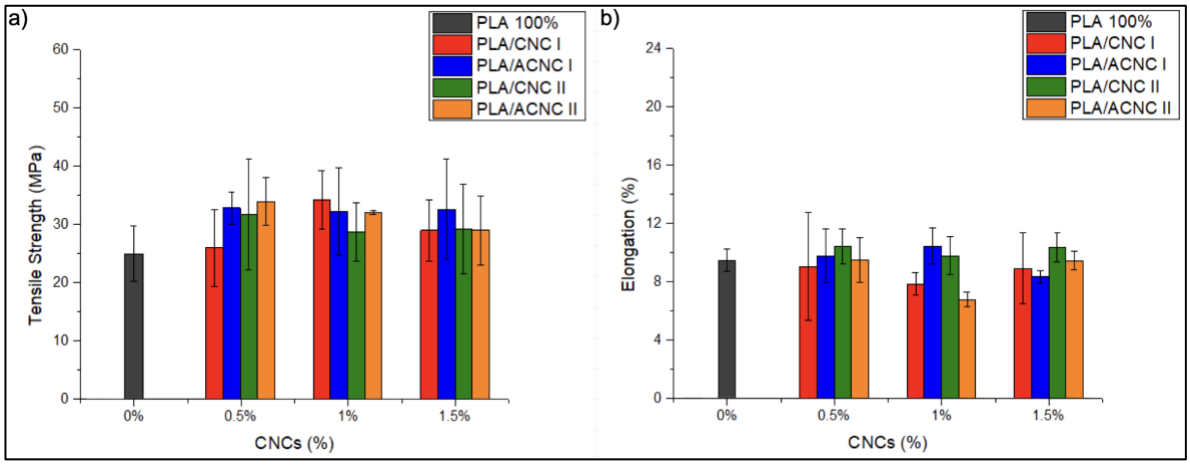

Figure 9. Graphical representation of the mechanical properties of neat PLA and PLA-based nanocomposite films as a function of nanoreinforcement content of a) tensile strength and b) elongation (mean ± SD, n = 5).

Table 8. Mechanical parameters (tensile strength, elongation and Young's modulus) for neat PLA and PLA-based nanocomposite films. Values are expressed as mean ± standard deviation (n = 5). An asterisk (*) indicates a value significantly different from neat PLA according to Dunnett's test (p < 0.05).

Samples (n = 5)	T. Strength (MPa)	Elongation (%)	Young´s Modulus (MPa)
PLA	25.07 ± 4.75	9.51 ± 0.80	280.23 ± 64.38
PLA/CNC I 0.5	26.16 ± 6.58	9.10 ± 3.72	265.40 ± 66.42
PLA/ACNC I 0.5	33.00 ± 2.80	9.84 ± 1.81	344.84 ± 70.80
PLA/CNC II 0.5	31.89 ± 9.54	10.45 ± 1.20	311.63 ± 119.22
PLA/ACNC II 0.5	34.09 ± 4.13	9.55 ± 1.51	364.32 ± 74.71
PLA/CNC I 1	34.39 ± 4.98	7.89 ± 0.78	438.17 ± 70.30
PLA/ACNC I 1	32.35 ± 7.62	10.50 ± 1.24	315.99 ± 109.89

PLA/CNC II 1	28.94 ± 4.96	9.83 ± 1.32	277.31 ± 50.94
PLA/ACNC II 1	32.17 ±0.33	6.83 ± 0.51	348.97 ± 108.51
PLA/CNC I 1.5	29.10 ± 5.34	8.96 ± 2.42	335.96 ± 78.11
PLA/ACNC I 1.5	32.75 ± 8.52	8.40 ± 0.44	390.76 ± 100.96
PLA/CNC II 1.5	29.33 ± 7.42	10.42 ± 1.02	268.62 ± 127.81
PLA/ACNC II 1.5	29.17 ± 6.13	9.50 ± 0.63	286.90 ± 47.05

CONCLUSIONS

This study demonstrates that cellulose polymorphism and surface acetylation are key determinants of the properties of eucalyptus kraft pulp-derived CNCs in PLA biocomposite films. Sulfuric acid hydrolysis of both native (cellulose I) and mercerized (cellulose II) kraft pulp yielded cellulose nanocrystals with similar crystallinity indices (70–74 %) and colloidal stability, while exhibiting marked differences in surface sulfur content, consistent with the distinct chain accessibility of each allomorph during hydrolysis. Heterogeneous acetylation under identical reaction conditions produced a substantially higher degree of substitution for ACNC II (DS = 1.38) relative to ACNC I (DS = 0.23), supporting the interpretation that the antiparallel chain arrangement of the cellulose II lattice facilitates reagent access to surface hydroxyl groups. Acetylation also resulted in partial desulfation of both variants, with expected benefits for thermal performance.

When incorporated into PLA films by solution casting, cellulose II-based nanocrystals consistently showed a greater tendency to promote PLA matrix crystallization than their cellulose I counterparts at equivalent loadings, as evidenced by both XRD and DSC analyses. Acetylation enhanced the apparent nucleating efficiency of CNC I formulations, possibly associated with improved compatibility with the casting solvent, though direct evidence of dispersion state was not obtained in this study, while its influence on CNC II was less pronounced given the already high crystallinity values promoted by the unmodified form. The higher matrix crystallinity in CNC II-based biocomposites was accompanied by improved thermal stability, with onset degradation temperatures up to 16 °C above neat PLA in selected

formulations, reflecting both a more ordered crystalline matrix and reduced sulfate group density following acetylation.

Mechanical evaluation revealed no statistically significant effects of nanocrystal type, loading, or their interaction on tensile strength or Young's modulus, with small effect sizes confirming the practical absence of reinforcement for these properties. A statistically significant reduction in elongation was detected exclusively at PLA/ACNC II 1.0 wt%, interpreted as an isolated finding consistent with high matrix crystallinity rather than a generalizable trend. These results indicate that the primary functional contribution of ACNC II is the tuning of PLA crystallinity and thermal stability, supporting the valorization of eucalyptus kraft pulp for sustainable packaging applications.

ACKNOWLEDGEMENTS

Cristóbal Donoso acknowledges financial support and scholarship from Dirección de Postgrado UdeC. The authors also acknowledged the VRID-UdeC Microscopy Laboratory for providing facilities and technical support for microscopy analyses.

V. CONCLUSIONES

El presente trabajo abordó la producción, modificación superficial e incorporación en matrices de PLA de nanocristales de celulosa de los polimorfos I y II derivados de pulpa Kraft blanqueada de eucalipto, con el propósito de determinar la influencia del polimorfismo celulósico y de la acetilación sobre las propiedades fisicoquímicas, estructurales, térmicas y mecánicas de los materiales biocompuestos resultantes. El uso de pulpa de eucalipto como materia prima enlaza el desarrollo de materiales avanzados con una de las cadenas productivas forestales más relevantes de Chile y Latinoamérica, abriendo una vía de valorización de alto valor agregado para los subproductos de la industria celulósica nacional.

En relación con la preparación y caracterización de los nanocristales, la hidrólisis ácida con ácido sulfúrico permitió obtener CNC I y CNC II con índices de cristalinidad comparables, confirmando que el tratamiento de mercerización previo logró la conversión del polimorfo nativo al regenerado sin comprometer de manera sustancial la fracción cristalina. La química superficial de ambos polimorfos mostró diferencias relevantes: CNC I presentó un mayor contenido de azufre superficial que CNC II, coherente con la distinta accesibilidad de sus redes cristalinas durante la hidrólisis, y ambas variantes exhibieron potenciales zeta negativos en un rango que sugiere una estabilidad coloidal aceptable en suspensión acuosa. La acetilación heterogénea generó grados de sustitución marcadamente distintos entre polimorfos, con un DS de 0,23 para ACNC I y de 1,38 para ACNC II, lo que respalda la hipótesis de que la disposición antiparalela de cadenas de la celulosa II confiere una mayor accesibilidad química a los grupos hidroxilo superficiales y favorece la incorporación de grupos acetilo bajo condiciones de reacción idénticas. Esta modificación se acompañó de una reducción parcial del contenido de grupos sulfato en ambos casos, con implicancias directas sobre el comportamiento térmico posterior de los materiales.

En cuanto a la influencia del polimorfismo y la acetilación sobre la cristalinidad de la matriz de PLA, los análisis de XRD y DSC mostraron tendencias consistentes indicando que los nanocristales de celulosa II tienden a actuar como agentes nucleantes más eficientes que sus contrapartes de celulosa I a cargas equivalentes, promoviendo elevados índices de cristalinidad en las películas biocompuestas. La acetilación potenció la capacidad nucleante de las formulaciones basadas en CNC I, probablemente mediante una mejor dispersión bajo las condiciones de colado en solución, mientras que su efecto sobre CNC II fue menos pronunciado, dado que el polimorfo no modificado ya inducía altos grados de cristalización. Los valores de grado de cristalinidad obtenidos por DSC, particularmente en las formulaciones con CNC II, se aproximan al límite teórico para PLA y deben interpretarse como cristalinidades aparentes empleadas principalmente para comparar tendencias relativas entre formulaciones, más que como indicadores de un estado plenamente cristalino. En conjunto, estos resultados posicionan al polimorfismo celulósico y a la modificación superficial como variables de diseño relevantes para modular la microestructura cristalina del PLA en sistemas procesados por solución.

En términos de estabilidad térmica, las formulaciones con CNC II y, especialmente, con ACNC II mostraron temperaturas de inicio de degradación superiores a las del PLA puro, con incrementos de hasta aproximadamente 16 °C en composiciones seleccionadas. Este comportamiento se asocia tanto al mayor ordenamiento cristalino de la matriz polimérica como a la reducción de grupos sulfato termolábiles tras la acetilación, aunque la contribución relativa de cada factor no fue desacoplada en este trabajo y constituye una oportunidad para investigaciones futuras orientadas a separar efectos de estructura cristalina y química superficial.

Respecto a las propiedades mecánicas, los resultados indicaron que el tipo de nanorefuerzo y su concentración tuvieron un efecto solo moderado sobre la resistencia a la tracción, el módulo de Young y la elongación. Las tendencias observadas apuntan a que el rango de carga de 0,5–1,0% en masa ofrece el mejor compromiso entre rigidez, resistencia y ductilidad, con ligeros incrementos en

resistencia y módulo y sin pérdidas severas de deformabilidad; sin embargo, las pruebas estadísticas no evidenciaron diferencias significativas entre formulaciones, por lo que estos cambios deben considerarse como tendencias no concluyentes más que como mejoras mecánicas firmemente demostradas. Bajo las condiciones de procesado empleadas, el principal beneficio funcional de los nanocristales acetilados de celulosa II se manifestó en el ajuste de la cristalinidad y de la estabilidad térmica de la matriz de PLA, mientras que el refuerzo mecánico fue, en el mejor de los casos, leve y estadísticamente no significativo.

Desde una perspectiva de aplicación, los materiales desarrollados en este trabajo resultan prometedores para el ámbito del embalaje sostenible de alimentos, particularmente en segmentos que requieren mayor estabilidad térmica que la del PLA puro, como el envasado en caliente o el almacenamiento a temperaturas moderadamente elevadas. El incremento de la cristalinidad y de la hidrofobicidad superficial de la matriz podría, además, contribuir a mejorar propiedades de barrera frente a gases y humedad, hipótesis que deberá ser verificada en estudios futuros mediante caracterización directa de dichas propiedades. La ruta de producción planteada, basada en pulpa Kraft de eucalipto y en etapas de modificación química relativamente accesibles, sugiere que la integración de estos nanomateriales como etapa de valor añadido dentro de una biorrefinería forestal es técnicamente plausible y coherente con las metas de desarrollo forestal sostenible a nivel nacional.

En conjunto, los resultados obtenidos confirman de manera robusta la parte de la hipótesis relativa a la mayor eficiencia de acetilación y a la capacidad nucleante superior de los nanocristales de celulosa II frente a los de celulosa I, y demuestran que la combinación de polimorfismo celulósico y acetilación permite ajustar de forma efectiva la cristalinidad y la estabilidad térmica de biocompuestos de PLA. En cambio, la propuesta de una mejora mecánica marcada solo se cumple parcialmente, ya que las diferencias observadas en resistencia, módulo y elongación se mantuvieron en rangos modestos y sin respaldo estadístico concluyente bajo las condiciones de este estudio. No obstante, el conjunto de evidencias generadas contribuye a cerrar una brecha de conocimiento sobre el

papel del polimorfismo celulósico en sistemas PLA/CNC y sienta bases para el diseño racional de biocompuestos de embalaje bio-basados a partir de recursos forestales renovables, con potencial de aportar a la transición hacia una bioeconomía forestal circular en el contexto chileno y latinoamericano.

VI. BIBLIOGRAFÍA

1. Abdallah, W., & Kamal, M. R. (2018). Influence of process variables on physical characteristics of spray freeze dried cellulose nanocrystals. *Cellulose*, *25*(10), 5711-5730. https://doi.org/10.1007/s10570-018-1975-0
2. Agbakoba, V. C., Hlangothi, P., Andrew, J., & John, M. J. (2023). Preparation of cellulose nanocrystal (CNCs) reinforced polylactic acid (PLA) bionanocomposites filaments using biobased additives for 3D printing applications [10.1039/D3NA00281K]. *Nanoscale Advances*, *5*(17), 4447-4463. https://doi.org/10.1039/D3NA00281K
3. Aguayo, M. G., Fernández-Pérez, A., Oviedo, C., Reyes, G., & Reyes-Contreras, P. (2020). Relationship between Structural Characteristics of Cellulose Nanocrystals Obtained from Kraft Pulp. *Nanomaterials*, *2020*, 1775. https://doi.org/10.3390/nano10091775
4. Agustin, M. B., Nakatsubo, F., & Yano, H. (2016). The thermal stability of nanocellulose and its acetates with different degree of polymerization. *Cellulose*, *23*(1), 451-464. https://doi.org/10.1007/s10570-015-0813-x
5. Al Hakkak, J., Grigsby, W. J., Kathirgamanathan, K., & Edmonds, N. R. (2019). Generation of Spherical Cellulose Nanoparticles from Ionic Liquid Processing via Novel Nonsolvent Addition and Drying. *Advances in Materials Science and Engineering*, *2019*(1), 2081027. https://doi.org/https://doi.org/10.1155/2019/2081027
6. Ávila Ramírez, J. A., Fortunati, E., Kenny, J. M., Torre, L., & Foresti, M. L. (2017). Simple citric acid-catalyzed surface esterification of cellulose nanocrystals. *Carbohydrate Polymers*, *157*, 1358-1364. https://doi.org/https://doi.org/10.1016/j.carbpol.2016.11.008
7. Bangar, S. P., Harussani, M. M., Ilyas, R. A., Ashogbon, A. O., Singh, A., Trif, M., & Jafari, S. M. (2022). Surface modifications of cellulose nanocrystals: Processes, properties, and applications. *Food Hydrocolloids*, *130*, 107689. https://doi.org/https://doi.org/10.1016/j.foodhyd.2022.107689
8. Bayat, P., Anstey, A., Dubé, M. A., Morse, T., Cunningham, M. F., & Meek, K. M. (2025). Effect of carboxylated cellulose nanocrystal acetylation on PLA nanocomposite crystallization behavior. *Composites Part C: Open Access*, *18*, 100673. https://doi.org/https://doi.org/10.1016/j.jcomc.2025.100673
9. Bolat, F., Necolau, M. I., Bîru, E. I., Zaharia, A., & Iovu, H. (2024). Comparative Analysis of Solvent Casting and Pickering Emulsion Techniques for Improving the Mechanical Properties of Surface-Modified Cellulose Nanomaterial-Reinforced Polylactic Acid Composites. *Polymers*, *16*(23), 3406.
10. Carrillo-Varela, I., Albornoz, M., Reyes-González, I., Aguayo, M. G., Elgueta, E., Reyes-Contreras, P., Pereira, M., & Mendonça, R. T. (2024). Tailoring cellulose-based hydrogels by phosphorylation of unbleached kraft pulps for adsorption applications. *Cellulose*, *31*(12), 7629-7660. https://doi.org/10.1007/s10570-024-06086-2
11. Carrillo-Varela, I., Pereira, M., & Mendonça, R. T. (2018). Determination of polymorphic changes in cellulose from Eucalyptus spp. fibres after alkalization. *Cellulose*, *25*(12), 6831-6845. https://doi.org/10.1007/s10570-018-2060-4
12. Chen, T., Li, J., Xu, J., Gao, Y., Zhu, S., Wang, B., & Ying, G. (2023). Effect of Acetylation of Two Cellulose Nanocrystal Polymorphs on Processibility and Physical Properties of Polylactide/Cellulose Nanocrystal Composite Film. *Molecules*, *28*(12), 4667.
13. Dhar, P., Gaur, S. S., Soundararajan, N., Gupta, A., Bhasney, S. M., Milli, M., Kumar, A., & Katiyar, V. (2017). Reactive Extrusion of Polylactic Acid/Cellulose Nanocrystal Films for Food Packaging Applications: Influence of Filler Type on

Thermomechanical, Rheological, and Barrier Properties. *Industrial & Engineering Chemistry Research*, *56*(16), 4718-4735. https://doi.org/10.1021/acs.iecr.6b04699
14. Dhar, P., Tarafder, D., Kumar, A., & Katiyar, V. (2015). Effect of cellulose nanocrystal polymorphs on mechanical, barrier and thermal properties of poly(lactic acid) based bionanocomposites [10.1039/C5RA06840A]. *RSC Advances*, *5*(74), 60426-60440. https://doi.org/10.1039/C5RA06840A
15. Dong, F., Yan, M., Jin, C., & Li, S. (2017). Characterization of Type-II Acetylated Cellulose Nanocrystals with Various Degree of Substitution and Its Compatibility in PLA Films. *Polymers (Basel)*, *9*(8). https://doi.org/10.3390/polym9080346
16. Duan, L., Liu, R., Duan, Y., Li, Z., & Li, Q. (2022). A simultaneous strategy for the preparation of acetylation modified cellulose nanofiber/polypropylene composites. *Carbohydrate Polymers*, *277*, 118744. https://doi.org/https://doi.org/10.1016/j.carbpol.2021.118744
17. Duchemin, B. (2015). Mercerisation of cellulose in aqueous NaOH at low concentrations. *Green Chemistry*, *17*(7), 3941-3947.
18. Dufresne, A. (2019). Nanocellulose Processing Properties and Potential Applications. *Current Forestry Reports*, *5*(2), 76-89. https://doi.org/10.1007/s40725-019-00088-1
19. Eichers, M., Bajwa, D., Shojaeiarani, J., & Bajwa, S. (2022). Biobased plasticizer and cellulose nanocrystals improve mechanical properties of polylactic acid composites. *Industrial Crops and Products*, *183*, 114981. https://doi.org/https://doi.org/10.1016/j.indcrop.2022.114981
20. Espino-Pérez, E., Bras, J., Ducruet, V., Guinault, A., Dufresne, A., & Domenek, S. (2013). Influence of chemical surface modification of cellulose nanowhiskers on thermal, mechanical, and barrier properties of poly (lactide) based bionanocomposites. *European Polymer Journal*, *49*(10), 3144-3154.
21. Ferro, M., Mannu, A., Panzeri, W., Theeuwen, C. H. J., & Mele, A. (2020). An Integrated Approach to Optimizing Cellulose Mercerization. *Polymers (Basel)*, *12*(7). https://doi.org/10.3390/polym12071559
22. Fortunati, E., Armentano, I., Zhou, Q., Iannoni, A., Saino, E., Visai, L., Berglund, L. A., & Kenny, J. M. (2012). Multifunctional bionanocomposite films of poly(lactic acid), cellulose nanocrystals and silver nanoparticles. *Carbohydrate Polymers*, *87*(2), 1596-1605. https://doi.org/https://doi.org/10.1016/j.carbpol.2011.09.066
23. French, A. D. (2021). Combining Computational Chemistry and Crystallography for a Better Understanding of the Structure of Cellulose. *Adv Carbohydr Chem Biochem*, *80*, 15-93. https://doi.org/10.1016/bs.accb.2021.11.002
24. Gan, L., Liao, J., Lin, N., Hu, C., Wang, H., & Huang, J. (2017). Focus on Gradientwise Control of the Surface Acetylation of Cellulose Nanocrystals to Optimize Mechanical Reinforcement for Hydrophobic Polyester-Based Nanocomposites. *ACS Omega*, *2*(8), 4725-4736. https://doi.org/10.1021/acsomega.7b00532
25. Gil-Castell, O., Reyes-Contreras, P., Barra, P. A., Teixeira Mendonça, R., Carrillo-Varela, I., Badia, J. D., Serra, A., & Ribes-Greus, A. (2022). The Role of Eucalyptus Species on the Structural and Thermal Performance of Cellulose Nanocrystals (CNCs) Isolated by Acid Hydrolysis. *Polymers*, *14*(3), 423.
26. Gong, J., Li, J., Xu, J., Xiang, Z., & Mo, L. (2017). Research on cellulose nanocrystals produced from cellulose sources with various polymorphs [10.1039/C7RA06222B]. *RSC Advances*, *7*(53), 33486-33493. https://doi.org/10.1039/C7RA06222B

27. Huntington, B., Pitcher, M. L., & Sheikhi, A. (2023). Nanoengineering the Redispersibility of Cellulose Nanocrystals. *Biomacromolecules*, *24*(1), 43-56. https://doi.org/10.1021/acs.biomac.2c00518
28. Jordan, J. H., Easson, M. W., & Condon, B. D. (2019). Alkali Hydrolysis of Sulfated Cellulose Nanocrystals: Optimization of Reaction Conditions and Tailored Surface Charge. *Nanomaterials (Basel)*, *9*(9). https://doi.org/10.3390/nano9091232
29. Kaduk, J. A., & Blanton, T. N. (2013). An improved structural model for cellulose II. *Powder Diffraction*, *28*(3), 194-199. https://doi.org/10.1017/S0885715613000092
30. Kusmono, Listyanda, R. F., Wildan, M. W., & Ilman, M. N. (2020). Preparation and characterization of cellulose nanocrystal extracted from ramie fibers by sulfuric acid hydrolysis. *Heliyon*, *6*(11), e05486. https://doi.org/10.1016/j.heliyon.2020.e05486
31. Lam, D.-N., Thien, D. V. H., Nguyen, C.-N., Nguyen, N. T. T., Van Viet, N., & Van-Pham, D.-T. (2022). Thermally stable cellulose nanospheres prepared from office waste paper by complete removal of hydrolyzed sulfate groups. *Carbohydrate Polymers*, *297*, 120009. https://doi.org/https://doi.org/10.1016/j.carbpol.2022.120009
32. Langan, P., Nishiyama, Y., & Chanzy, H. (2001). X-ray Structure of Mercerized Cellulose II at 1 Å Resolution. *Biomacromolecules*, *2*(2), 410-416. https://doi.org/10.1021/bm005612q
33. Lee, J. H., Park, S. H., & Kim, S. H. (2020). Surface Alkylation of Cellulose Nanocrystals to Enhance Their Compatibility with Polylactide. *Polymers*, *12*(1), 178.
34. Li, W., Cai, G., & Zhang, P. (2019). A simple and rapid Fourier transform infrared method for the determination of the degree of acetyl substitution of cellulose nanocrystals. *Journal of Materials Science*, *54*(10), 8047-8056. https://doi.org/10.1007/s10853-019-03471-2
35. Li, W., Li, W., Xiong, Z., & Zhang, P. (2024). Controllable acetylation of cellulose nanocrystal by uniform design and response surface methodology. *Carbohydr Polym*, *333*, 121990. https://doi.org/10.1016/j.carbpol.2024.121990
36. Lim, C. S. S., Chan, E. W. C., Lee, H. C., & Wong, C. W. (2025). Hydrophobic modification of cellulose nanocrystals refined via non-fuming process from Leucaena leucocephala. *Polymer Bulletin*, *82*(13), 8193-8211. https://doi.org/10.1007/s00289-025-05799-z
37. Lin, N., Huang, J., Chang, P. R., Feng, J., & Yu, J. (2011). Surface acetylation of cellulose nanocrystal and its reinforcing function in poly (lactic acid). *Carbohydrate Polymers*, *83*(4), 1834-1842.
38. López, D., Aguayo, M. G., Núñez-Decap, M., Reyes-Contreras, P., Teixeira Mendonça, R., Reyes-González, I., Opazo, B., & Valdebenito, F. (2025). Synthesis and Characterization of Phosphorylated Cellulose Nanocrystals: Exploring Factors for Enhanced Thermal and Colloidal Stability. *Polymers*, *17*(19), 2581.
39. Ma, T., Hu, X., Lu, S., Cui, R., Zhao, J., Hu, X., & Song, Y. (2021). Cellulose nanocrystals produced using recyclable sulfuric acid as hydrolysis media and their wetting molecular dynamics simulation. *International Journal of Biological Macromolecules*, *184*, 405-414. https://doi.org/https://doi.org/10.1016/j.ijbiomac.2021.06.094
40. Mariano, M., El Kissi, N., & Dufresne, A. (2014). Cellulose nanocrystals and related nanocomposites: Review of some properties and challenges. *Journal of Polymer Science Part B: Polymer Physics*, *52*(12), 791-806. https://doi.org/https://doi.org/10.1002/polb.23490

41. Mechernene, N., Benkraled, L., Zennaki, A., Arabeche, K., Berrayah, A., Mechernene, L., Bouriche, A., Benabdellah, S. A., Bouberka, Z., Barrera, A., & Maschke, U. (2026). A Novel Plasticization Mechanism in Poly(Lactic Acid)/PolyEthyleneGlycol Blends: From Tg Depression to a Structured Melt State. *Polymers*, *18*(3), 317.
42. Melchor-Martínez, E. M., Macías-Garbett, R., Alvarado-Ramírez, L., Araújo, R. G., Sosa-Hernández, J. E., Ramírez-Gamboa, D., Parra-Arroyo, L., Alvarez, A. G., Monteverde, R. P. B., Cazares, K. A. S., Reyes-Mayer, A., Yáñez Lino, M., Iqbal, H. M. N., & Parra-Saldívar, R. (2022). Towards a Circular Economy of Plastics: An Evaluation of the Systematic Transition to a New Generation of Bioplastics. *Polymers (Basel)*, *14*(6). https://doi.org/10.3390/polym14061203
43. Nagarajan, S., Skillen, N. C., Irvine, J. T., Lawton, L. A., & Robertson, P. K. (2017). Cellulose II as bioethanol feedstock and its advantages over native cellulose. *Renewable and Sustainable Energy Reviews*, *77*, 182-192.
44. Nagarajan, V., Zhang, K., Misra, M., & Mohanty, A. K. (2015). Overcoming the Fundamental Challenges in Improving the Impact Strength and Crystallinity of PLA Biocomposites: Influence of Nucleating Agent and Mold Temperature. *ACS Applied Materials & Interfaces*, *7*(21), 11203-11214. https://doi.org/10.1021/acsami.5b01145
45. Nishiyama, Y., Langan, P., & Chanzy, H. (2002). Crystal Structure and Hydrogen-Bonding System in Cellulose Iβ from Synchrotron X-ray and Neutron Fiber Diffraction. *Journal of the American Chemical Society*, *124*(31), 9074-9082. https://doi.org/10.1021/ja0257319
46. Nofar, M., Sacligil, D., Carreau, P. J., Kamal, M. R., & Heuzey, M.-C. (2019). Poly (lactic acid) blends: Processing, properties and applications. *International Journal of Biological Macromolecules*, *125*, 307-360. https://doi.org/https://doi.org/10.1016/j.ijbiomac.2018.12.002
47. Oberlintner, A., Likozar, B., & Novak, U. (2023). Effect of Environment on Acetylated Cellulose Nanocrystal-Reinforced Biopolymers Films. *Polymers (Basel)*, *15*(7). https://doi.org/10.3390/polym15071663
48. Omran, A. A. B., Mohammed, A., Sapuan, S. M., Ilyas, R. A., Asyraf, M. R. M., Rahimian Koloor, S. S., & Petrů, M. (2021). Micro- and Nanocellulose in Polymer Composite Materials: A Review. *Polymers (Basel)*, *13*(2). https://doi.org/10.3390/polym13020231
49. Park, S., Baker, J. O., Himmel, M. E., Parilla, P. A., & Johnson, D. K. (2010). Cellulose crystallinity index: measurement techniques and their impact on interpreting cellulase performance. *Biotechnology for biofuels*, *3*(1), 10.
50. Peng, S., Luo, Q., Zhou, G., & Xu, X. (2021). Recent Advances on Cellulose Nanocrystals and Their Derivatives. *Polymers*, *13*(19), 3247.
51. Potenza, M., Bergamonti, L., Lottici, P. P., Righi, L., Lazzarini, L., & Graiff, C. (2022). Green Extraction of Cellulose Nanocrystals of Polymorph II from Cynara scolymus L.: Challenge for a "Zero Waste" Economy. *Crystals*, *12*(5), 672.
52. Rahimi Kord Sofla, M., Batchelor, W., Kosinkova, J., Pepper, R., Brown, R., & Rainey, T. (2019). Cellulose nanofibres from bagasse using a high speed blender and acetylation as a pretreatment. *Cellulose*, *26*(8), 4799-4814. https://doi.org/10.1007/s10570-019-02441-w
53. Rana, A. K., Frollini, E., & Thakur, V. K. (2021). Cellulose nanocrystals: Pretreatments, preparation strategies, and surface functionalization. *International Journal of Biological Macromolecules*, *182*, 1554-1581. https://doi.org/https://doi.org/10.1016/j.ijbiomac.2021.05.119
54. Rashid, A. B., Hoque, M. E., Kabir, N., Rifat, F. F., Ishrak, H., Alqahtani, A., & Chowdhury, M. E. H. (2023). Synthesis, Properties, Applications, and Future Prospective of Cellulose Nanocrystals. *Polymers*, *15*(20), 4070.

55. Reyes-González, I., Carrillo-Varela, I., Mazega, A., Tarrés, Q., Delgado-Aguilar, M., & Mendonça, R. T. (2024). Chemo-enzymatic pre-treatment of eucalyptus kraft pulp for phosphorylated nanocellulose production. *Cellulose*, *31*(18), 10931-10949. https://doi.org/10.1007/s10570-024-06257-1
56. Ryoo, J., Oh, D. X., & Park, J. (2025). Engineering Poly(Lactic Acid)/Cellulose Nanocrystal Composites: A Comparative Review of Preparation Strategies and their Influence on Structure-Property Relationships. *Advanced Sustainable Systems*, *9*(10), e00654. https://doi.org/https://doi.org/10.1002/adsu.202500654
57. Scherrer, P. (1918). Bestimmung der Größe und der inneren Struktur von Kolloidteilchen mittels Röntgenstrahlen. *Nachrichten von der Gesellschaft der Wissenschaften zu Göttingen, Mathematisch-Physikalische Klasse*, *1918*, 98-100. http://eudml.org/doc/59018
58. Shin, H., Thanakkasaranee, S., Sadeghi, K., & Seo, J. (2022). Preparation and characterization of ductile PLA/PEG blend films for eco-friendly flexible packaging application. *Food Packaging and Shelf Life*, *34*, 100966. https://doi.org/https://doi.org/10.1016/j.fpsl.2022.100966
59. Spinella, S., Re, G. L., Liu, B., Dorgan, J., Habibi, Y., Leclere, P., Raquez, J.-M., Dubois, P., & Gross, R. A. (2015). Polylactide/cellulose nanocrystal nanocomposites: Efficient routes for nanofiber modification and effects of nanofiber chemistry on PLA reinforcement. *Polymer*, *65*, 9-17.
60. Sukmawan, R., Kusmono, & Wildan, M. W. (2023). Optimizing Acetic Anhydride Amount for Improved Properties of Acetylated Cellulose Nanofibers from Sisal Fibers Using a High-Speed Blender. *ACS Omega*, *8*(30), 27117-27126. https://doi.org/10.1021/acsomega.3c02178
61. Sullivan, E. M., Moon, R. J., & Kalaitzidou, K. (2015). Processing and Characterization of Cellulose Nanocrystals/Polylactic Acid Nanocomposite Films. *Materials*, *8*(12), 8106-8116.
62. Sun, L., Zhang, X., Liu, H., Liu, K., Du, H., Kumar, A., Sharma, G., & Si, C. (2021). Recent advances in hydrophobic modification of nanocellulose. *Current Organic Chemistry*, *25*(3), 417-436.
63. Trivedi, A. K., & Gupta, M. K. (2024). PLA based biodegradable bionanocomposite filaments reinforced with nanocellulose: development and analysis of properties. *Scientific Reports*, *14*(1), 23819. https://doi.org/10.1038/s41598-024-71619-5
64. Trivedi, A. K., Gupta, M. K., & Singh, H. (2023). PLA based biocomposites for sustainable products: A review. *Advanced Industrial and Engineering Polymer Research*, *6*(4), 382-395. https://doi.org/https://doi.org/10.1016/j.aiepr.2023.02.002
65. Vatansever, E., Arslan, D., & Nofar, M. (2019). Polylactide cellulose-based nanocomposites. *International Journal of Biological Macromolecules*, *137*, 912-938. https://doi.org/https://doi.org/10.1016/j.ijbiomac.2019.06.205
66. Wang, Q., Ji, C., Sun, J., Zhu, Q., & Liu, J. (2020). Structure and Properties of Polylactic Acid Biocomposite Films Reinforced with Cellulose Nanofibrils. *Molecules*, *25*(14). https://doi.org/10.3390/molecules25143306
67. Wang, S., Wang, Q., & Kai, Y. (2022). Cellulose nanocrystals obtained from microcrystalline cellulose by p-toluene sulfonic acid hydrolysis, NaOH and ethylenediamine treatment. *Cellulose*, *29*(3), 1637-1646. https://doi.org/10.1007/s10570-021-04409-1
68. Wi, J., Choi, J., & Lee, S. H. (2025). PLA-Based Biodegradable Polymer from Synthesis to the Application. *Polymers (Basel)*, *18*(1). https://doi.org/10.3390/polym18010121

69. Wu, Z., Xu, J., Gong, J., Li, J., & Mo, L. (2018). Preparation, characterization and acetylation of cellulose nanocrystal allomorphs. *Cellulose*, *25*(9), 4905-4918. https://doi.org/10.1007/s10570-018-1937-6
70. Xu, J., Wu, Z., Wu, Q., & Kuang, Y. (2020). Acetylated cellulose nanocrystals with high-crystallinity obtained by one-step reaction from the traditional acetylation of cellulose. *Carbohydrate Polymers*, *229*, 115553. https://doi.org/https://doi.org/10.1016/j.carbpol.2019.115553
71. Yoo, Y., & Youngblood, J. P. (2016). Green one-pot synthesis of surface hydrophobized cellulose nanocrystals in aqueous medium. *ACS Sustainable Chemistry & Engineering*, *4*(7), 3927-3938.
72. Yu, F., Fei, X., He, Y., & Li, H. (2021). Poly(lactic acid)-based composite film reinforced with acetylated cellulose nanocrystals and ZnO nanoparticles for active food packaging. *International Journal of Biological Macromolecules*, *186*, 770-779. https://doi.org/https://doi.org/10.1016/j.ijbiomac.2021.07.097
73. Zhao, J., Zhao, Y., Wang, Z., & Peng, Z. (2016). Effect of polymorphs of cellulose nanocrystal on the thermal properties of poly(lactic acid)/cellulose nanocrystal composites. *The European Physical Journal E*, *39*(12), 118. https://doi.org/10.1140/epje/i2016-16118-2
74. Zlenko, D. V., Vtyurina, D. N., Usachev, S. V., Skoblin, A. A., Mikhaleva, M. G., Politenkova, G. G., Nikolsky, S. N., & Stovbun, S. V. (2021). On the orientation of the chains in the mercerized cellulose. *Scientific Reports*, *11*(1), 8765. https://doi.org/10.1038/s41598-021-88040-x